MARTIN MARIETTA ENERGY SYSTEMS LIBRARIES
3 4456 0360444 6

[redacted]

ORNL-435
PHYSICS-GENERAL

AEC RESEARCH AND DEVELOPMENT REPORT

DECLASSIFIED
CLASSIFICATION CHANGED TO:
BY AUTHORITY OF
BY

LABORATORY RECORDS

ORNL SUMMER SHIELDING SESSION

Gale Young, Leader

NEUTRON AND GAMMA ATTENUATION THROUGH TUNGSTEN CARBIDE AND BORON CARBIDE

W. K. ERGEN
C. E. CLIFFORD

OAK RIDGE NATIONAL LABORATORY
CENTRAL RESEARCH LIBRARY
DOCUMENT COLLECTION
LIBRARY LOAN COPY
DO NOT TRANSFER TO ANOTHER PERSON
If you wish someone else to see this document, send in name with document and the library will arrange a loan.
UCN-7969
(3 3-67)

OAK RIDGE NATIONAL LABORATORY
OPERATED BY
CARBIDE AND CARBON CHEMICALS CORPORATION
FOR THE
ATOMIC ENERGY COMMISSION

OAK RIDGE, TENNESSEE

[redacted]

[redacted]

ORNL-435

This document consists of 72 pages. Copy 7 of 124 copies. Series A.

Contract No. W-7405, eng. 26 *

ORNL SUMMER SHIELDING SESSION

Gale Young, Leader

NEUTRON AND GAMMA ATTENUATION THROUGH TUNGSTEN CARBIDE AND BORON CARBIDE

W. K. Ergen and C. E. Clifford

Participating Personnel:

T. I. Arnette	ORNL	J. G. Puckett	NEPA
E. P. Blizard	ORNL	J. C. Sellers	NEPA
J. M. Cassidy	ORNL	H. P. Sleeper, Jr.	G.E.
C. E. Clifford	ORNL	G. Thornton	NEPA
W. K. Ergen	NEPA	W. E. White	NEPA
M. S. Johnson	NEPA		

DATE ISSUED:

DEC - 9 1949

OAK RIDGE NATIONAL LABORATORY
OPERATED BY
Carbide and Carbon Chemicals Corporation
for the
Atomic Energy Commission
Post Office Box P
Oak Ridge, Tennessee

(It is intended to issue this report also as NEPA-1136-STR-14)

[redacted]

*Explanation on Page 3.

MARTIN MARIETTA ENERGY SYSTEMS LIBRARIES

3 4456 0360444 6

[redacted]

ORNL 435
Physics-General

OAK RIDGE NATIONAL LABORATORY INTERNAL DISTRIBUTION:

1. G. T. Felbeck (C&CCC)
2-3. 706-A Library
4. 706-B Library
5. Biology Library
6. Health Physics Library
7-8. Training School Library
9-12. Central Files
13. J. A. Swartout
14. J. H. Gillette
15. A. Hollaender
16. J. H. Frye, Jr.
17. E. J. Murphy
18. C. N. Rucker
19. W. D. Lavers
20. A. M. Weinberg
21. A. A. Lane
22. A. N. Lyon
23. M. M. Mann
24. C. E. Larson (Y-12)
25. W. B. Hume (K-25)
26. C. E. Clifford
27. E. P. Blizard
28. W. K. Ergen
29-36. Central Files (Off-Area)

OAK RIDGE NATIONAL LABORATORY EXTERNAL DISTRIBUTION:

37-48. Argonne National Laboratory
49. Armed Forces Special Weapons Project
50-51. Atomic Energy Commission, Washington
52. Battelle Memorial Institute
53-56. Brookhaven National Laboratory
57-58. Bureau of Ships
59-62. Carbide and Carbon Chemicals Corp. (K-25)
63-66. Carbide and Carbon Chemicals Corp. (Y-12)
67. Columbia University (Dunning)
68-71. General Electric Company, Richland
72. Hanford Operations Office
73. Iowa State College
74-77. Knolls Atomic Power Laboratory
78-81. Los Alamos
82-84. Mound Laboratory
85. National Advisory Committee for Aeronautics
86-87. National Bureau of Standards
88. Naval Radiological Defense Laboratory
89. NEPA Project
90. New Brunswick Laboratory
91-94. New York Operations Office
95. North American Aviation, Inc.
96. Patent Branch, Washington
97. Sandia Laboratory
98-112. Technical Information Branch, ORE
113. UCLA Medical Research Laboratory (Warren)
114-118. University of California Radiation Laboratory
119-120. University of Rochester
121-124. Westinghouse Electric Corporation

[redacted]

[redacted]

This report is one of a series on shielding and represents part of the work of a summer group working principally at Oak Ridge National Laboratory. Participants are drawn from Nuclear Development Associates (Navy contract), NEPA, Bureau of Ships and Bureau of Aeronautics (Navy Department), AEC, RAND, General Electric, Argonne and Oak Ridge National Laboratory

[redacted]

[redacted]

TABLE OF CONTENTS

	Page
Abstract	5
Neutron and Gamma Attenuation Through Tungsten Carbide and Boron Carbide	6
Appendix I - General Remarks	11
Appendix II - Experimental Facilities and Equipment	13
Appendix III- Gamma Data	18
Appendix IV - Neutron Attenuation Data	24
Appendix V - Neutron Traverses	33
Literature	36
Tables	38
Figures	58

[redacted]

[redacted]

ORNL-435

ABSTRACT

Gamma and neutron attenuation was measured through WC, B_4C, and hydrogenous material, in various geometries (figure 1). The gamma attenuation curves are summarized in figure 2 and the neutron attenuation curves in figure 3. For samples, the composition of which is given in tables 1 and 2, we found the gamma and neutron relaxation lengths and related data summarized in tables 3 and 4.

[redacted]

[redacted]

NEUTRON AND GAMMA ATTENUATION THROUGH TUNGSTEN CARBIDE AND BORON CARBIDE

W. K. Ergen and C. E. Clifford

A. General

Exploratory experiments were carried out as a joint ORNL-NEPA program on neutron and gamma attenuation in various combinations of tungsten carbide, boron carbide, and hydrogenous material. Because of the rush character of the experiments and the limitations of the facility (which has since been improved) the results have to be viewed with some reservation.

The facility used was the "core hole" in the ORNL pile, a rectangular opening in the pile shield, into which the sample was inserted in the form of rectangular slabs. Disturbing boundary effects at the boundary between the pile shield and the sample were aggravated by streaming of radiation through the unavoidable clearances around the sample, in spite of the fact that this streaming was minimized by varying the core hole cross section in steps, thus interrupting line of sight propagation of radiation.

Figure 1 gives a summary of the geometries investigated and tables 1 and 2 give a summary of the compositions of some of the shield samples.

B. Gamma Data

The results of the gamma measurements are plotted in Figure 2. The three geometries investigated for gamma attenuation were:

(1) Run 36: 152 g/cm^2 of B_4C, followed by 230 g/cm^2 of WC, and a thin outer layer of B_4C. This run gave the gamma ray attenuation through B_4C (assuming that the secondary gammas due to the neutron flux are negligible). It also

[redacted]

[redacted]

gave the gamma attenuation through WC, without the influence of secondaries, as the neutrons had been attenuated in the B_4C layer. No significant deviations from a straight exponential is noticed in the WC layer through the attenuation measured.

(2) Runs 37 and 40: A 175 g/cm^2 layer of WC was close to the inside*) of the shield and produced secondary gammas. The apparent relaxation weight is now not much less than for B_4C, but this depends on the neutron conditions. The WC layer was followed by 130 g/cm^2 of B_4C, which attenuated the neutrons. The outside layer of 150 g/cm^2 of WC essentially attenuated only the secondary gammas created in the inside layer, since the primary gammas were practically eliminated in this inside layer, and no neutrons were left to create secondaries in the outside layer. The relaxation weight for the secondaries was found to be larger than the relaxation weight found for the primaries in run 36.

(3) Run 44: Alternating layers of WC and B_4C were used. The inside part of the sample had a greater WC:B_4C ratio than the outside part. The relaxation weight for the outside part came out almost equal to the relaxation weight of pure B_4C. The results of the run are particularly doubtful.

The relaxation weights for gammas, determined in these four runs, are tabulated in table 3, together with the attenuations over which the measurements have been carried out.

C. Neutron Data

The results of representative neutron attenuation measurements are plotted in figure 3 . The geometries investigated were:

---

*) "Inside" or "front" is the side closer to the pile.

[redacted]

[redacted]

(1) Run 36: (See above). The neutron attenuation curve measured with gold foils goes into a straight exponential, after an initial drop corresponding to the elimination of thermal neutrons. (These results were checked in run 39.)

(2) Run 45:*) Indium threshold detector measurements in B_4C show a fast neutron relaxation length which is only slightly longer than the relaxation length measured with gold foils.

(3) Runs 37 and 40: (See above). Measurement of the neutrons with Au and W foils shows very little decrease of the foil activation through the inside layer of WC. This indicates a very slight decrease of the capture gamma generation as one proceeds through this layer.

Measurement with 3 MeV aluminum threshold detectors shows a neutron relaxation length of 4.1 to 5.1 cm through WC of theoretical density. The uncertainty in the relaxation length is mainly due to the uncertainty on how much the aluminum present contributed to the attenuation. The attenuation weight is much better determined. See table 4.

The attenuation through the B_4C following the WC is, at first, much more rapid than the attenuation measured in run 36, and referring to the "virgin" neutrons which have not passed through WC. However, eventually the attenuation curve goes into an exponential with a relaxation length of the virgin neutrons. Describing the initial, fast attenuation as an effect of the WC, H. P. Sleeper [1] obtained a WC neutron relaxation length in good agreement with the relaxation length obtained with threshold detectors.

(4) Run 42: Alternating layers of B_4C and WC, with higher WC concentration on the inner part of the sample. The relaxation length of material compressed to

---

*) Not shown in figure 3.

[redacted]

theoretical density is plotted against the B_4C concentration in figure 4. If the relaxation length of a mixture could be computed as the average of the relaxation lengths of the components, one would get a straight line. The minimum seems to indicate that the computation of the relaxation length is not as simple, but the simple averaging computation has been used in shield weight calculations so far. The experiments in themselves are not significant enough to establish the non-validity of the averaging rule, but one can think of theoretical reasons why the averaging rule should break down.

(5) Run 43: Hydrogenous material. All runs with hydrogenous material are of doubtful value due to holes in the paraffin which were discovered too late. The attenuation curve seems to flatten out as one proceeds to large sample thicknesses.

(6) Run 38 and 41: Alternating layers of B_4C and Paraffin. The attenuation curve flattens out as one proceeds to large sample thicknesses. Foils inserted into the paraffin layer got 10^2 - 10^3 times more active than those inserted in B_4C at a corresponding sample thickness. This emphasizes the large number of capture gammas in heavy material surrounded by moderator, as compared to the number of capture gammas in heavy material protected by boron. This has possibly some bearing on hydrides as shielding material.

The relaxation lengths and relaxation weights for neutrons and the attenuation factor through which they have been measured are tabulated in table 4.

D. Neutron Traverses

The neutron flux was also measured at points off the axis. These "traverses" indicate that the influx of neutrons from the sides of the sample falsified the results at large sample thicknesses and the parts of the sample for which

[redacted]

the data are believed to be unreliable and for this reason are shown as ····· lines on the top of figure 3. Typical traverses are shown in figure 5. It is interesting to note that the neutron influx from the top is much larger than from the bottom which is due to the larger gap at the top. This gap was only about 1" and not line-of-sight all the way through, and still it had such in large effect. Quantitative data would have been very valuable because of the implication for gas-filled ducts and voids.

[redacted]

[redacted]

APPENDIX I

General Remarks

The reactor shielding experiments described in this report were carried out as a joint project of Oak Ridge National Laboratory and the NEPA Division of the Fairchild Engine & Airplane Corporation. The tests were performed with NEPA material at the ORNL core hole shield testing facility, with both organizations furnishing personnel.

The experiments were exploratory in nature and the results should be viewed with some reservation, partly because of the rush character of the project and partly because of the limitations of the testing facility itself. Change of samples, some background measurements and standardization procedures required pile shutdowns, and these shutdowns were not always available. Also, measurements with small sample thicknesses were connected with high radiation levels and hence the measuring time had to be reduced at the expense of statistical reliability, in order to prevent over-exposure of personnel. The new lid tank facility will be essentially free from these limitations.

During the experiments, interim reports were issued[2]. Not all necessary corrections had been included in these interim reports and where they differ from the present summary, the summary data are more reliable.

Preparatory to writing the present report, the data were assembled in a series of memos from the present authors to R. L. Echols. A list of these memos is found in the list of references [3]. It may be noted that the "NEPA" run number used in these memos is equal to the run number used in this report, minus 35.

The description of the core hole facility is contained in ORNL-32 [4].

[redacted]

[redacted]

Detailed items preculiar to the "NEPA" test are contained in the memos listed as reference [5], the last of these memos being a summary of the earlier memos.

The present summary report omits some of the details contained in the above references. Copies of the NEPA memos are available from Don Cowen, NEPA Division, Fairchild Engine and Airplace Corporation, P. O. Box 415, Oak Ridge, Tennessee.

[redacted]

[redacted]

APPENDIX II

Experimental Facilities and Equipment

As mentioned, the tests were carried out in the "core hole" at the ORNL pile. Only the three largest steps of this hole were used. A steel transport box was constructed for each of these 3 steps (see fig. 6). Frames fitted into these transport boxes. The frames were covered with aluminum foil and filled with either boron carbide or tungsten carbide. The transport boxes ride on small wheels, which roll on tracks. This facilitated the insertion of the heavy loaded transport boxes into the core hole.

For the purpose of this project the steps of the core hole are numbered, 1 through 4, inclusive, from the inside*) face out. The step #1 was not used. The transport boxes were numbered 2, 3 and 4, according to the step into which they fitted.

The three transport boxes were made of cold rolled steel. Top, bottom and sides are of 5/8" thick material. Front and back are 1/4" thick. (See fig. 6). The wheels were countersunk in the bottom of the sample. It was believed that the innermost face of the #2 transport box would become very radioactive if exposed to the slow neutron flux emerging from the pile. Hence, a 1/16" layer of "boron paint" was applied to this face. The "boron paint" was made up of equal parts of B_4C powder, glyptal cement, and glyptal thinner.

During the experiments, the #2 transport box still got rather radioactive, particularly on the sides. Hence, a second transport box was constructed to fit the #2 step, with the idea of using the two #2 transport boxes alternatingly, and to avoid the necessity of loading frames into a transport box, which just came out of the test hole and had been made strongly radioactive.

---

*) "Inside" or "in front" means on the side closer to the pile.

[redacted]

[redacted]

It may be mentioned that the main part of the activity seemed to decay with the 2.59 hr Mn half life, rather than the long iron half life, though no exact measurements have been made regarding the decay time. In any case, after a short cooling down period, the transport box could easily be loaded again.

The second #2 transport box did have boron coatings on the sides, and the top and bottom as it was hoped to eliminate in this way the influx of slow neutrons from the sides of the shielding test sample. No boron coating was applied at the inner face and the outer face of the box.

The frames were made of steel plates for the sides, bottom and top, with aluminum cover plates in front and back. The steel plates were about 3/8" thick.

The frames were marked with a W or B, depending on whether they were filled with WC or B_4C. They further carried a two digit number. The first digit indicates the core hole step for which the frame was designed and the second digit distinguishes from each other the frames containing the same material and designed for the same step.

The outline of the frames is shown in fig. 7, which also gives a list of the dimensions of the frames. The height and width is the same for all frames fitting into the same step. The thicknesses given do not include the aluminum covers. Each of these covers--and there are two for each frame--were 1/8" thick for WC filled frames and 1/16" for the B_4C filled ones. For the WC frames, bulging of the aluminum covers was avoided by the use of spacers which connected two covers. These spacers were arranged in such a way that there was little alignment of the spacers of adjacent frames. No such spacers were used in the B_4C frames. The spacers are indicated in fig. 7, by ● .

The tungsten carbide and boron carbide used had a density of less than the theoretical density. For the B_4C, the density amounted to 1.9 ± 0.05 (theo-

[redacted]

[redacted]

retical density 2.54) and for WC to 7.9 $\pm$ 0.1 (theoretical 15.7) except for the frames W-41 and W-42 which had a density of 8.35. These densities are computed from the total weight of B_4C or WC, and the inside volume of the frames. They are thus average densities.

The low densities were chosen because it was hoped to minimize the streaming of radiation from the X-shield into the test sample. It was expected that both tungsten carbide and boron carbide of theoretical densities would have better attenuation properties than the cement of the X-shield, and a material of less than theoretical density than would match the cement. Of course, perfect matching would require the simultaneous matching of the relaxation lengths for neutrons of all energies, and γ-rays of all energies, and that obviously could not be obtained by adjusting the one variable -- density -- alone.

Fig. 7 also gives the g/cm^2 for each of the carbide filled frames or "slabs", using the average density as computed above. These g/cm^2 values again do not include the Al covers.

Great care was taken during the loading of the slabs in order to obtain the low densities of material uniformly over each slab. However, the slabs were used for a considerable number of experiments, and concern was felt for possible settling or shifting. Hence, after conclusion of the experiment the density distribution in the slabs was checked by visual inspection, and also by means of γ-ray transmission.

The visual inspection was done after taking off the top of the frames. The WC had settled by 1/4" - 1", depending on the frame.

For the γ-ray transmission measurement, a radium source was moved over one surface of the slab and a "cutie-pie" ionization chamber over the other. The source and the chamber always were in a line perpendicular to the slab and as

[redacted]

[redacted]

close to the surface as possible. Over any given slab, the "cutie-pie" reading varied by 20% and more, not counting the large variation occurring when the "cutie-pie" approached the top of the slab.

The boron carbide used was commercial grade abrasive "Norbide". The frames were very uniform in density when scanned with the Ra source. These frames were opened for visual inspection and no appreciable settling or packing was noted.

The foils were mounted in a geometry shown in fig. 8 on masonite slabs, at least in the earlier experiments. These masonite slabs were 1/4" thick and were milled out at the positions of the foils in order to facilitate the insertion of cadmium covers for the foils. In later experiments, the masonite foil holders were sometimes replaced by aluminum strips which supported the foils and which were fastened on the slabs with scotch tape. These strips were made of .005" aluminum and were used between non-hydrogenous slabs in order to avoid perturbations by the hydrogenous material. The distances between the foils on the aluminum strips are the same as on the masonite holders unless noted otherwise.

The arrangement of a foil in the sample is defined by its "location" and "position". The "location" refers to the distance of the foil from the inner face of the sample and can be seen from the geometry drawings of the detailed reports. The "position" gives the vertical and sidewise displacement of the foil, and is indicated by a code number, 1 through 15, as shown in fig. 8.

The foils used were of gold, tungsten, indium and aluminum. Gold was mostly used but tungsten was used in a few runs to give an idea of the capture γ's to be expected in tungsten at various locations. Indium and aluminum acted as treshold detectors.

[redacted]

[redacted]

In general, the results of the foil measurements were quoted in saturated counts/min KW, which means the counts/min, which would have been obtained immediately after an infinite exposure at 1 KW pile power.

γ measurements were taken by introducing the γ-sensitive instrument behind the shielding test plug, and by varying the number of slabs in the plug between measurements. This is in contrast to the neutron foil measurements where the whole plug was exposed at one time and remained unchanged during the measurement, and where the foils were distributed inside the plug. Generally, the test plugs were built up by inserting the innermost slabs first, and by then adding the other slabs in the order from the inside to the outside.

Measuring instruments were a GM tube, the standard health physics cutie-pie and a crystal scintillation counter. The latter was used only in runs 5 and 9.

The GM tube and the crystal counter were collimated with the idea that they could "see" only the test sample, and not the walls of the core hole.

The various geometries used are shown schematically in fig. 1. Details, like masonite foil holders, have been omitted, but they can be seen from the tables giving the neutron attenuations.

[redacted]

[redacted]

APPENDIX III

Gamma Data

The gamma attenuation through boron carbide and tungsten carbide has been investigated in various geometries. In run 36, a thick layer of B_4C was followed by a layer of WC, and finally some more B_4C was added. No appreciable production of secondary gammas could take place in the WC, as the neutrons had been strongly attenuated in the first thick layer of B_4C.

In runs 37 and 40, the WC was placed in front of the B_4C, in order to determine the relative importance of the production of secondary gammas in tungsten carbide. Only a thin (2") layer of B_4C was placed in front of the WC to prevent the WC from getting so radioactive that it could not be handled. However, this thin B_4C was omitted in one experiment of run 40, and then the pile was operated a low power. This permitted a study of the importance of the thin B_4C layer on secondary gamma production.

In run 44, alternating layers of WC and B_4C were used to allow a comparison with the neutron attenuation of run 42, having a similar geometry.

Details of the geometries are described in NEPA Memos STRM-20, STRM-28, STRM-26 and STRM-31, and the main features of these geometries can be seen from fig. 1 and tables 5-7, in particular column 1. For each run, this column gives the material added between two successive measurements, the first line in this column being the thinnest sample measured. The total thickness of the sample, expressed in cm and g/cm^2 is found in columns 3 and 4 for each run. This total thickness is obtained by adding up the cm*) or g/cm^2 of the material listed in column 1, up to the location in question. It may be noticed that the extraneous material, such as the iron of the transport boxes, the masonite of the foil

*) Actual dimension, not the dimension obtainable by compression to theoretical density.

[redacted]

[redacted]

holders, and the aluminum of the covers of the slabs has been included. This extraneous material amounted to quite a bit in some cases, f.i. 1/4" of Al plus 1/4" of masonite for 2" of WC. Hence the densities, as computed by dividing the g/cm^2 by the cm, differ from the densities quoted in Appendix II. No allowance was made, however, for such local perturbations as the foils, the cadmium covers over the foils, or the milled out parts of the foil holders.

Column 4 in tables 5-7, and the graph figure 2, contain, unless otherwise specified, the counts/min on the GM tube, divided by the pile power at the time of measurement.

The GM tube was the main measuring instrument, but it could not be used at points very close to the inner face of the shield because the fluxes got too high there. At these points, the crystal counter or the cutie-pie were used, and these measurements were normalized to the GM data by taking measurements at points within the range of both the GM tube and the other instrument. Then the cutie-pie or crystal data were multiplied by such a factor as to coincide with the GM data at these points. The GM data of runs 36, 37 and 40 have been normalized so that the same counting rate corresponds to the same γ-flux (for details and uncertainties see STRM-31). However, no such normalization was possible for run 44. Hence, only the slope of the run 44 curve should be compared with the slope of the other runs, but the ratio of run 44 readings and readings of the other runs is not significant, except as to order of magnitude.

It may be seen, that the data for run 36 fall essentially on 3 straight lines, on semilog paper. The first and last of these lines apply to the B_4C, and correspond to 48.5 g/cm^2 for a factor of e or 111 g/ cm^2 for a factor of 10 (measured between 58 g/cm^2 and 152 g/cm^2). The first point at 23 g/cm^2 has not

[redacted]

[redacted]

been considered in this computation, as it seems to deviate from the straight line, either because of a measuring error, or because the "equilibrium" has not been reached that close to the inner shield surface. If this first point were included, the attenuation would amount to a factor of e for 45 g/cm^2. The medium straight line applies to the WC and gives 27 g/cm^2 for a factor of e or 62 g/cm^2 for a factor of 10. (Measured between the points 152 g/cm^2 and 382 g/cm^2.)

In runs 37 and 40, the attenuation through the first layer of WC is less than in the WC of run 1. For runs 37 and 40, the average attenuation through the first WC layer amounts to 41 g/cm^2 for a factor of e or 94 g/cm^2 for a factor of 10 (measured between 101 and 196 g/cm^2). This is not much better attenuation than obtained with B_4C in run 36, and the reason is the production of secondary gammas by the neutrons. The attenuation through the B_4C layer is not well-determined because of the uncertainty of the normalization between the run 37 and the run 40 data. However, within this uncertainty the B_4C attenuation checks with the value obtained in run 36.

The slope of the attenuation curve through the WC in the outer part of the run 37 sample (between 329 g/cm^2 and 442 g/cm^2) corresponds to 30.7 g/cm^2 for a factor of e, which is less attenuation than obtained in WC in run 36 This may not be significant because of the uncertainty in calibration of the GM tube, but it would indicate a difference in hardness of the capture gammas prevailing in run 37 as compared with the pile gammas prevailing in run 36. Here the last point, at 479 g/cm^2, had not been included in the computation, because it seemed high compared to the straight line extrapolation of the values obtained from the other points, and because readings at the low countings rates are unreliable.

[redacted]

[redacted]

Had this point been included, the attenuation by a factor of e would require 32.8 g/cm^2.

It may be noted that between points A and B (329 and 382 g/cm^2) the samples of runs 36 and 37 contain about the same materials in about the same amounts, but the distribution of the B_4C and WC is different in the two runs. (For run 36, these points fall into the #4 transport box, and include about 10 g/cm^2 more iron than the corresponding points for run 37. This is the largest difference in the materials contained in runs 36 and 37, but it is still rather unimportant). Between A and B the intensity in run 37 is about 5 times the value it obtained in run 36, indicating the importance of the capture gammas.

In run 44, a distinction can be made between the data referring to the #2 transport box and the data of the #3 box, because of the varying thickness of the WC and the B_4C slabs. The points of the #2 box were fitted by a straight line, which shows a relaxation weight of 36 g/cm^2 (83 g/cm^2 for a factor of 10). The points of the #3 box were also fitted by a straight line, which gives a relaxation weight of 46 g/cm^2 (106 g/cm^2 for a factor of 10), about as much as pure B_4C. It should be remembered, that the measurements in the #2 box were primarily carried out with the crystal counter, and those in the #3 box with the GM tube. Hence, there might have been a difference between the two boxes in the spectrum measured. Furthermore, the background measurements, which affect the relaxation length in the #3 box, are not too certain. The above figures should hence be regarded with some reservation.

Table 3 summarizes the data on the gamma attenuation. Some arbitrariness was unavoidable in the table. The first column gives the main component of the shield. Details of the composition are recorded in table 1. The densities listed in the third column are the actual, not the theoretical, densities of the main components, not including the extraneous materials like masonite foil

[redacted]

[redacted]

holders, etc. The range of attenuation is obtained as the ratio of two numbers. The denominator is in any case the lowest reading used in the computation of the relaxation weight (column 5). If the component in question extends essentially to the inside of the shielding sample (as the B_4C in run 36) than the attenuation curve is extrapolated, as a straight exponential to zero sample thickness. The extrapolated value for zero sample thickness is used as the numerator, on the theory that the sample in front of the first actual reading contributes to the establishment of the spectrum. If the component in question does not extend anywhere near to the innerface of the sample, as the WC in runs 36 and 37, then the numerator is the highest reading used in the computation of the relaxation weight. This procedure is adopted because it was used by Sleeper in ORNL-436. In run 44, the extrapolated value for zero sample thickness is used in the computation of the attenuation range for the #2 transport box and also for the #3 transport box. This seems justified because the material in front of the #3 box was very similar to the material in the #3 box, itself, and probably established about the same spectrum as the #3 box material would have done in the same location.

Table 1, shows the composition in milligram atom/cc, of the samples for which we quoted the relaxation weights in table 3. The iron of the transport boxes has not been included because it was concentrated in one or two spots and not distributed throughout the sample. However, masonite foil holders and aluminum covers were considered. In run 44, the first and the last B_4C slab in the #2 transport box was not included because this makes the #2 comparable in geometry to the #3 box, each having alternating layers of B_4C and WC, starting

[redacted]

[redacted]

with a WC layer and ending with a B_4C layer. The densities assumed for B_4C and WC in the computation are the actual densities (1.9; 7.9 or 8.35) and not the theoretical ones. The other densities are: Wood, 0.7; masonite, 1.2; paraffin, 0.9. The composition of masonite and wood are assumed to be described by the empirical formula $C_6H_{10}O_5$, and the composition of paraffin by CH_2.

In run 40, a comparison was made between the gamma rays obtained with the innermost B_4C slab in the test sample and with this slab omitted. In either case, the measurements were taken behind the #2 transport box, containing the geometry shown in table 6 behind the innermost B_4C slab. The #3 and #4 transport boxes were not in the test hole in either case. The gamma intensity proved to be twice as high without the B_4C slab than with it. It has to be remembered that even without the B_4C slab, there were 1/4" of iron and 1/8" of aluminum between the WC and the pile.

[redacted]

[redacted]

APPENDIX IV

Neutron Attenuation Data

The neutron attenuation data are summarized in tables 8-16 , and in figures 9-14 . The tables are quite analogous to the tables 5-7 . The C means cadmium covered foils. The attenuation curves became less reliable at large attenuations because of streaming, which is shown by ------lines.

Whereas the tables are arranged in the order of the run numbers, the figures are used to combine similar data for easier comparison.

Table 16 and figure 9 refer to run 45. The sample was essentially B_4C, and indium foils were used. These foils are activated by neutron capture to a 54 min and a 48 day activity, and fast neutrons above about 0.5 MEV induce a 4.5 hr activity. The decay of the foil activity was followed for several days and the decay curves were analyzed into the above 3 half lives and the counts/min at the end of the exposure were recorded in table 16 and figure 9 . The 54 min half life points fall quite well on a straight exponential with a 7.3 cm relaxation length and the 48 day curve proceeds practically parallel to this exponential, but the fast neutron attenuation length, as indicated by the line for the 4.5 hour activity shows a relaxation length of 7.8 cm. This difference in relaxation length for the different neutron energies is just on the border of the experimental error.

Figure 10 shows the data on the 54 min activity of run 45 combined with the data of runs 36 (table 8) and 39 (table 11).

The common feature of these 3 runs is the B_4C which constituted the major component of the material in the portion of the sample for which data are avail-

[redacted]

able for all three runs.

Run 36 differs from the other two runs by the use of masonite foil holders, whereas the foils of run 39 and 45 were mounted on aluminum strips. Run 45 used indium foils, whereas run 36 and 39 used gold foils. Run 39 used 1 cm^2 foils, whereas the two other runs used 25 cm^2 foils.

The data of run 39 had been multiplied by a factor of 40, which had previously been found to be the conversion factor between 1 cm^2 and 25 cm^2 gold foils. This conversion factor takes care of the difference in size of the foils, and also of the fact that the smaller foils were somewhat further away from the GM tube during counting than the large foils. It indicates that, under the counting procedure used, a large foil gives 40 times the counting rate of a small foil, if both foils were exposed to the same flux for the same time.

No similar conversion factor is available between the indium and gold foils of the same size. In fact, this conversion factor can be expected to depend on the neutron spectrum, as the indium and gold cross-sections will vary differently with neutron energy. Division of the indium saturated counts/min by the pile power would, however, give almost the same value as obtained with gold at the same location. This is more or less accidental. In order to prevent superposition of the data of runs 45 and 36, the indium data were arbitrarily divided by 1000, rather than by the pile power.

It may be seen that the attenuation through the first slab of B_4C is very great, corresponding to the elimination of slow neutrons. Even through the second slab, the attenuation in run 36 and 45 is somewhat larger than through the rest of the shield. Though there is some scattering of the points on the plot, the data for all three runs can be fitted very well by exponentials having a

[redacted]

relaxation length of 7.3 cm. This relaxation length has been measured through an attenuation factor of about 1500. If compressed to theoretical density, the sample would have a relaxation length of 5.5 cm, depending slightly on what assumptions are made on the contribution of the extraneous material (Al, masonite). The main uncertainty results from the small attenuation which had been measured.

It may be noted that the curve for run 36 proceeds by a factor of about 2.5 above the curve for run 39. This factor may be explained by the hydrogenous foil holders, used in the run 36, but its absolute value should not be regarded as well established because of the uncertainty in the conversion factor 40 between small and large gold foils.

The measurements for run 36 have also been taken through a layer of WC, which followed the thick layer of B_4C. The measurement in the WC layer show an irregular behavior, inasmuch as they first increase with increasing shield thickness, and, only after they pass through a flat maximum, can a decrease be noted. This increase in neutron flux is connected with a strong curvature of the traverses, but this alone hardly explains the behavior of the neutron flux. Reflexion of neutrons and softening of the spectrum due to the absence of boron are other possible explanations.

Figure 11 shows the results of runs 37 and 40. Here, one slab of B_4C was followed by WC, and then some more B_4C was added. In run 37, this B_4C was followed by more WC, but in run 39 only a little hydrogenous material was added at the outside in order to fill up the transport box. The main difference between the two runs consists in the use of masonite foil holders in run 37 and aluminum foil holders in run 40.

[redacted]

[redacted]

We find again the steep decrease at the beginning due to the absorption of thermal neutrons. Then there is the more flat course through WC followed by a steep decline in the B_4C. The increase at the tail end of the curve for run 40 is due to the hydrogenous material and run 37 shows the same increase of the readings in the WC as did run 36.

Figure 11 also contains the data on readings with tungsten foils, taken during run 40. The counts/min have not been reduced to "infinite exposure, at 1 KW pile power". The tungsten foil curve has the same shape as the gold foil curve though the two curves do not run exactly parallel.

The purpose of the tungsten foils was the determination of capture gammas in tungsten through the WC layer. The catch in this determination is the fact that only two tungsten isotopes (W^{184} and W^{186}) lead to activities which were measured in our experiments. The other isotopes -- noticeably W^{183} which certainly contributes a great deal to the capture gammas -- do not contribute to the measured activation of the foils. As to order of magnitude, it is fair to assume that the measured activity is always proportional to the total capture gammas, for all locations. With this assumption, it may be seen that the capture gammas decrease only by a factor of 5 through the WC layer of 175 g/cm^2. The primary gammas would be attenuated in this layer by a factor of 660 assuming a relaxation weight of 27 g/cm^2.

An attempt was also made to determine the attenuation of fast neutrons through the WC layer. The 10 min. activity induced in Al foils was used for this purpose. The attenuation measured in this way through the WC layer amounts to a factor of 13, or a relaxation length of 9.2 cm for the actual density used.

[redacted]

If the WC were compressed to theoretical density leaving the Al the way it is, the relaxation length would be 5.1 cm, and if it were assumed that the Al does not contribute appreciably to the neutron attenuation, the relaxation length through pure WC of theoretical density would be 4.1 cm.

H. P. Sleeper[1)] has determined the neutron relaxation length in WC from the data of run 40 by regarding this run as a Borst type experiment. Good agreement was found with the above quoted value.

The neutron data of run 42 (alternating B_4C and WC slabs) fall into two groups. Group 1 refers to the foils on the outerface of a B_4C slab and the innerface of a WC slab, and group 2 refers to the foils on the outerface of a WC slab and the innerface of a B_4C slab. Group 1 gives lower readings than group 2, but if the group 1 measurements are multiplied by 1.2, an almost smooth curve can be drawn through the data of both groups. This curve is shown in figure 12.

The curve shows a definite break which coincides with the boundary between the #2 and #3 transport boxes. Due to the different thicknesses of the B_4C and WC slabs, the ratio of boron to tungsten atoms was different in the two transport boxes. It amounted to 3.3 in the #2 box and to 5.6 in the #3 box. Regarding details in the computation of this ratio, see page 32. The relaxation length for the #2 box was computed between locations 3 and 9, and the relaxation length for the #3 box between locations 11 and 17. Then we obtain for the #2 and #3 transport boxes, respectively; 8.6 cm and 7.0 cm for the relaxation lengths of material of actual density; 5.6 cm and 4.7 cm for the relaxation length of the material of theoretical density, including the Al, 4.9 cm and 4.2 cm for the relaxation length of material of theoretical density, assuming that the aluminum did not help in the attenuation; and 42 g/cm^2 and 29 g/cm^2 for the relaxation

[redacted]

weight, including the aluminum.

Figure 4 , shows a plot using as abscissa the number of W atoms divided by the sum of the number of W atoms, plus the number of boron atoms. The ordinate is the relaxation length of theoretical density material. The point for "pure" WC is not quite comparable to the three other points, as it was measured by different methods. However, even the three comparable points indicate that the relaxation length of a mixture is not given as the average of the relaxation lengths of the components. If the latter were the case, as assumed in present methods of shield design, a straight line would be obtained in figure 4.

The experiments plotted in figure 4 are, by themselves, not conclusive enough to prove the fact that the relaxation length of a mixture of WC and B_4C is less than the average of the relaxation lengths of the components, and even less than the relaxation lengths of the pure components. However, this is not unreasonable on theoretical grounds.

If substantiated by further experiments, the short relaxation length for the mixture would have considerable influence on an optimum shield, both on the method of design and the final weight.

For comparison, figure 12 shows also the gamma date of run 44.* It may be seen that the gamma relaxation length in the #2 box is shorter than the neutron relaxation length, but the difference is hardly significant due to the uncertainty of the gamma data. In the #3 box, the relaxation length is shorter for the neutrons than for the gammas; hence, there seems to be too little heavy material in the #3 box composition, at least as far as the equalization of neutron and gamma relaxation length is concerned. From the neutron viewpoint alone, as

* The readings behind WC slabs have been multiplied by a suitable normalization factor, in order to make the line through these readings coincide with the line through the readings behind the B_4C slabs.

[redacted]

pointed out above, the #3 box composition seems to be close to an optimum. Hence, there might be a conflict between the various criteria for optimization.

Figure 13 , shows the neutron attenuation of run 43. This run used hydrogenous material, mostly paraffin. Unfortunately, the paraffin had some holes which were not noticed during the experiment, but the presence of which can be inferred from the traverses. These holes caused considerable scattering of the points around a smooth curve and decreased the value of the results. After an initial portion ascribable to the transition of the incident spectrum to the spectrum appropriate to the shielding sample, the attenuation curve seems to take a slightly concave shape, flattening out at higher attenuations. The average relaxation length, measured between 24.8 and 75.6 cm, amounts to 7.0 cm.

Figure 14 shows the data of runs 38 and 41. These runs used alternating layers of B_4C and paraffin, each layer being about 4" to 6" thick. The measuring foils were embedded in the center of each layer. Various troubles were encountered in run 38 and the data of run 41 seem more reliable, though both runs suffer under the uncertainty caused by the holes in the paraffin.

A difference between run 38 and 41 consisted in the fact that the front layer was paraffin in run 38, and B_4C in run 41. Furthermore, the hydrogenous layers in run 38, transport box 3, were about 6" thick, that is, as thick as the B_4C layers in this box, whereas in run 41 the paraffin slabs in box 3 were only 4" thick.

In run 38, gold foils and tungsten foils were used, some cadmium covered and some uncovered. This gives four kinds of foils. Obviously, only one kind could be employed as the center foil, and the data for the other foils were computed,

[redacted]

[redacted]

as described in the detailed report, from foils in the vicinity of the center foils.

No great importance should be attached to the ratio between the counts of the tungsten foils to the gold foils. This ratio depends on the counter used, due to the different hardness of the tungsten and gold radiation.

The cadmium covers were only used in the paraffin, as there were no large fluxes of thermal neutrons in the B_4C part of the sample. In the paraffin, a cadmium ratio of 13 was obtained.

In figure 14 smooth curves were drawn through each group of "corresponding foils", the groups being: uncovered gold foils in paraffin, Cd covered gold foils in paraffin, uncovered tungsten foils in paraffin, cadmium covered tungsten foils in paraffin, uncovered gold foils in B_4C and uncovered tungsten foils in B_4C. (The last group contains only one measured point; the other foils in this group gave unmeasurably low counting rates).

It may be noticed that these curves run approximately, but not exactly, parallel. Remarkable is the large ratio between the points for "uncovered foils in paraffin", and "uncovered foils in B_4C". This ratio lies between 400 and 1000. This indicates that heavy materials, if inserted into hydrogenous material, give a very much higher yield of secondary gammas than if embedded in boron. This may have some bearing on the question of heavy metal hydrides and their use in shields.

Furthermore, it may be noted that the curves all have a tendency of flattening out. This is in accordance with results obtained with other shields containing hydrogenous laminations alternating with laminations of some other material. In

[redacted]

[redacted]

our tests and in some of the others, this could be due to streaming of neutrons through holes in the sample. Regarding our tests, an inspection of the traverses shows streaming from the X-shield into the sample. This streaming is worse in run 38 than in run 41. In accordance with this, the curves of run 41 proceed steeper than those of run 38. In view of the strong tendency of the attenuation curves to flatten out at higher attenuations, no relaxation length can be quoted for this combination of materials.

Table 4 summarizes the neutron relaxation lengths and relaxation weight. The table is quite analogous to table 3 . The density quoted is the density of the main component, without consideration of the extraneous material. Since the relaxation length and relaxation weight includes the extraneous material, the ratio between these two quantities is not exactly equal to the density quoted. The details on the sample composition is given in table 2 , which is analogous to table 1 . The portion over which the attenuation curve exhibits its initial bend is included in the composition calculation in all cases in which the straight exponential and the initial bend occur in the same material (runs 36, 39, 43 and 45).

In run 42, the first B_4C slab in the #2 transport box was not included because this makes the #2 box comparable in geometry with the #3 box, each having alternating layers of B_4C and WC, starting with a WC layer and ending with a B_4C layer.

[redacted]

[redacted]

APPENDIX V

Neutron Traverses

The neutron measuring foils were arranged in crosses, as discussed earlier, in order to obtain information regarding the neutron flux at points off the center line of the test sample. In particular, they served as a check on how much the center line measurements might have been influenced by the streaming of neutrons from the X-shield into the sample or vice versa.

Tables 17-24 give the average saturated counts/min KW*) for the foils at the various locations and positions. Cadmium covered foils are marked with a C; W indicates a tungsten foil. Regarding the location, refer to the neutron attenuation tables. Regarding the position, see figure 8.

Since the #1 step of the core hole was not used in the tests, the sample started about 20" behind the inner face of the X-shield. At that depth, the neutrons in the X-shield seem to be attenuated already by a factor of 1000 [6], whereas the neutrons impinging on the test sample are essentially the unattenuated pile neutrons. Hence, close to the inner face of the test sample, there should be a higher neutron flux inside the sample than in the X-shield. This would result in convex traverses (high spot in middle) and in an outflux of neutrons from the sample into the shield, resulting in measured attenuations which are greater than the actual ones.

The samples tested were far more efficient shields than the X-shield, and the attenuation in the sample soon "caught up" with the attenuation in the

*) For run 39, the multiplication by the factor 40 (See p. 25) has not been carried out for the traverse data.

[redacted]

[redacted]

X-shield. Hence, at greater depth, the neutron flux in the test samples is less than the flux in the X-shield, the traverses can be expected to look concave (minimum in the middle), there would be an influx of neutrons in the test sample, and the measured relaxation length would be longer than the ones actually representative for the material.

The situation is somewhat complicated by various facts. In the first place, the transport boxes had to be designed somewhat smaller than the core hole. This left an air gap around the transport boxes, through which radiation could stream. Furthermore, the slabs had to be somewhat smaller than the transport boxes leaving additional airspace. Even if there had been no clearance, the iron of the core hole lining, of the transport boxes, and of the frames of the slabs constituted material of different neutron transmission properties than either the X-shield or the shielding sample.

Further complications arise from the settling of the material in the slabs, in particular the WC slabs. This introduces another airgap on top of the sample, varying in size between 1/4" and 1". The density of the slabs also was not quite uniform, and this might have somewhat influenced the distribution of the neutron flux over the traverses.

No attempt has been made to analyze the above complicated situation in a quantitative manner. The following examples, however, may illustrate the above points qualitatively. Further details on the traverses are contained in the detailed reports. While the detailed reports show the traverses one by one, and plotted on an expanded linear scale, this report plots all vertical traverses

[redacted]

[redacted]

for one run on one graph, and the present report further uses log paper in order to make all traverses readable on the same graph.

The first example is shown in fig. 5, representing the vertical traverses of run 43. This run used hydrogenous material (paraffin) only (see fig. 1). One can clearly see the maxima in the middle of the innermost traverse, and the minima in the middle of the traverses in the outer layer. (In addition, there are a few irregularities in the traverses due to inhomogeneities in the paraffin). Up to and including location 8, the traverses proceed fairly horizontal in the middle, and the data at the center do not seem to be influenced too much by the streaming. Starting with the next traverse (location 13) the streaming is obviously rather pronounced, and the data can no longer be regarded as reliable. It is also noticeable, that the readings on the up side of the traverse are higher than on the lower side. This is due to the larger airspace at the top.

Another interesting fact is illustrated by the vertical traverses of run 40 (fig. 15). Here it is evident, that the traverse shows a maxima in the middle and high spots on the sides, with minima between the middle and the sides. This shape was noticed in very many traverses. It is also remarkable that this shape becomes more pronounced as one proceeds from the inside to the outside of the WC-layer of the run 40 test sample. (Compare fig. 1). The effect is of the order of magnitude one would expect from the density variations in the slabs but attempts to correlate the individual traverses with the density variations in the individual slabs have been unsuccessful.

[redacted]

[redacted]

-References -

1) H. P. Sleeper - A Critical Review of ORNL Shield Measurements: Neutron Attenuation. (ORNL-436).

2) ORNL-228 - Physics Division Progress Report for the Quarter September, October, November, 1948. p. 71 ff.

W. K. Ergen, R. W. Coyle, and G. Thornton - The "NEPA" Bulk Shielding Tests, Nov. 8, 1948, NEPA 814-STR-8, Included in Shielding Symposium, Sept. 27-30, 1948, Supplement No. 1, issued by ORNL.

Letter to ORNL, E. P. Blizard, from W. K. Ergen, dtd 2/25/49 - Shield Testing Subsection Meeting at Brookhaven.

3) STRM-18 - Neutron Attenuation Through Alternating Layers of WC and B_4C (NEPA Run 7).

STRM-19 - Attenuation of Fast and Slow Neutrons Through Boron Carbide (NEPA Run 10).

STRM-20 - Neutron Attenuation Through B_4C, Followed by WC (NEPA Run 1, Gold Foil Data).

STRM-22 - Neutron Attenuation Through Paraffin (NEPA Run 8).

STRM-23 - Neutron Attenuation Through B_4C Without Hydrogenous Material (NEPA Run 4).

STRM-24 - Neutron Attenuation Through Alternating Layers of B_4C and Hydrogenous Material (Paraffin) (NEPA Run 6).

STRM-25 - Neutron Attenuation Through Alternating Layers of Hydrogenous Material and B_4C (NEPA Run 3).

STRM-26 - Neutron Attenuation Through WC (NEPA Run 5, Tungsten and Gold Foils).

STRM-27 - Neutron Attenuation Through WC (NEPA Run 5, Threshold Detectors).

STRM-28 - Neutron Attenuation Through WC Followed by B_4C (NEPA Run 2)

STRM-31 - Gamma Attenuation Through WC and B_4C (NEPA Runs 1, 2, 5 and 9)

STRM-34 - Errata in Memos on the 1948 NEPA Bulk Shielding Tests.

4) E. P. Blizard, C. E. Clifford, J. Cassidy - Shielding Efficiency of an Oxychloride--Iron Concrete--Comparison with Hanford Shield (ORNL-32, dtd 6/7/48 - See particularly p. 3, section on Testing Facility and Fig. 9).

5) W. K. Ergen, R. W. Coyle, G. Thornton - The NEPA Bulk Shielding Tests (NEPA 814-STR-8, dtd 11/8/48)

R. E. Githens and R. W. Coyle (NEPA) Memo to W. J. Koshuba, dtd 2/8/49 - Materials Used in Bulk Shielding Experiments.

R. E. Githens (NEPA) Memo to W. K. Ergen, dtd 3/1/49

[redacted]

[redacted]

Memo from W.K.Ergen and C.E.Clifford to E.P.Blizard "Experimental Facilities and Equipment used in the 1948 "NEPA" Bulk Shielding Tests," July 20, 1949. ORNL Central Files No. 49-8-80.

(6) E. P. Blizard. Reactor Shielding With an Iron Aggregate Concrete. Comparison with Ordinary Concrete. ORNL-209.

[redacted]

[redacted]

TABLE 1

Composition of Gamma Shielding Samples

Run #	Elemental Components (milligram atoms/cc)						
	H	B	O	Al	C	W	Total
36, B_4C	6.2	121.2	3.1	4.7	34.0	0	169.2
36, WC	7.3	0	3.6	11.8	36.5	32.0	91.2
37, WC	8.3	0	4.2	11.3	36.3	31.3	91.4
44, Box 2	0	62.0	0	8.4	34.2	18.7	123.3
44, Box 3	0	78.6	0	7.7	33.8	14.2	134.3

TABLE 2

Composition of Neutron Shielding Samples

Run #	Elemental Components (milligram atoms/cc)						
	H	B	O	Al	C	W	Total
36	7.2	117.5	3.6	4.9	33.7	0	166.9
39	0	129.6	0	5.9	32.4	0	167.9
45	0	130.3	0	5.2	32.6	0	168.1
37	5.6	0	2.8	10.0	36.7	33.3	88.4
40	0	0	0	10.7	36.0	36.0	82.7
42 Box 2	0	62.0	0	8.4	34.2	18.7	123.3
42 Box 3	0	78.6	0	7.7	33.8	14.2	134.3
43	116.9	0	5.5	0	59.5	0	181.9

[redacted]

[redacted]

TABLE 3

SUMMARY OF GAMMA ATTENUATION DATA

Shield	Run #	Density * g/cc	Range of Attenuation	Relaxation Weight g/cm^2	Remarks & References
B_4C	36	1.9	20	48	STRM-31
WC	36	7.9	5×10^3	27	STRM-31
WC	37	7.9	40	31	Secondary gammas, STRM-31
B_4C,WC	44	5.0	10^3	36	3.3 atoms B per atom W, STRM-31
B_4C,WC	44	4.2	10^5	46	5.6 atoms B per atom W, STRM-31

TABLE 4

SUMMARY OF NEUTRON ATTENUATION DATA

Shield	Run #	Density* g/cc	Range of Attenuation	Relaxation cm	Length g/cm^2	Remarks & References
B_4C	36	1.9	1500	7.3	15	STRM-20
B_4C	39	1.9	100	7.3	15	STRM-23
B_4C	45	1.9	3000	7.3	15	STRM-19
WC	40	7.9	13	9.2	68	STRM-26
B_4C,WC	42	5.0	1000	8.6	42	3.3 atoms B per atom W, STRM-18
B_4C,WC	42	4.2	10^5	7.0	29	5.6 atoms B per atom W, STRM-18
Paraffin	43	.9	4×10^4	7.0		STRM-22

* See page 32

[redacted]

[redacted]

RUN 36 | TABLE 5 | ORNL-435

GAMMA ATTENUATION

Sample Added	Location	Cms.	Gms/cm^2	Counts Min.Kw
½" Fe; ½" Mas. B-21, 1/8" Al	1	7.9	23.	7725. *
B-22, B-23, B-24, 3/8" Al, 3/4"Mas.	2	26.0	58.	3040. *
B-25, B-26, B-31, ½"Mas, ½"Fe, 3/8"Al.	3	46.8	107.	1095.
B-32, ¼" Mas, 1/8" Al.	4	54.9	122.	847.
B-33, 1/8" Al.	5	62.3	137.	585.
B-34, 1/8" Al, ¼" Mas.	6	70.4	152.	441.
W-31, ¼" Mas. ¼" Al.	7	76.0	190.	121. 108.
W-32, ¼" Mas. ¼" Al.	8	81.7	228.	29. 22.
W-33, ¼" Mas. ¼" Al.	9	87.3	265.	7.8 6.6
W-34, ¼" Al.	10	92.3	302.	1.8
W-41, ½" Fe. ¼" Mas. ¼" Al.	11	98.7	347.	.24
W-42, ¼" Mas. ¼" Al.	12	103.9	382.	.086
B-41, B-42, ¼" Al.	13	117.1	409.	.051

* Cutie pie normalized

[redacted]

RUN 40

TABLE 6

GAMMA ATTENUATION

Sample Added	Location	Cms.	Gms/cm^2	Counts Min.Kw
½" Fe., B-22, W-21, W-22, 5/8" Al.	1	17.9	101.	731
W-23, 1/4" Al.	2	23.9	149.	201
W-24, 1/4" Al.	3	30.2	196.	71
B-26, B-25, 1/4" Al.	4	41.0	218.	33
B-24, B-23, B-21, 3/8" Al.	5	57.2	251.	15
RUN 37				
1/2" Fe; 2" Mas. B-26, W-21, W-22, W-23, W-24, B-25, B-24, B-23, B-22, B-21; 1-3/4" Al.	1	62.2	258.	14
1/2" Mas. 1/2" Fe., B-31, 1/8" Al.	2	72.3	284.	8.2
B-32, B-33, 1/4" Mas., 1/4" Al.	3	87.7	314.	3.9
B-34, 1/8" Al., 1/4" Mas.	4	95.8	329.	2.7
W-31, 1/4" Al., 1/4" Mas.	5	101.4	367.	.80
W-32, 1/4" Al., 1/4" Mas.	6	107.1	405.	.23
W-33, 1/4" Al., 1/4" Mas.	7	112.7	442.	.068
W-34, 1/4" Al.	8	117.7	479.	.028

RUN 44

TABLE 7

GAMMA ATTENUATION

Sample Added	Location	Cms.	Gms/cm^2	Counts Min.Kw
½" Fe. B-25, W-23, 3/8" Al.	1	13.0	68.	1405 **
B-24, 1/8" Al.	2	18.3	79.	1032 **
W-22, ¼" Al.	3	23.9	119.	240 **
B-23, 1/8" Al.	4	29.2	131.	200 **
W-24, B-22, 3/8" Al	5	40.9	189.	60 **
W-21, B-21, B-26, ½" Al	6	57.1	251.	7.5 **
¼" Mas. Felt, ½" Fe. W-31, ¼" Al.	7	64.0	299.	2.3
B-32, 1/8" Al	8	71.6	314.	1.7
W-32, ¼" Al.	9	76.5	351.	.85
B-31, 1/8" Al	10	84.1	365.	.58
W-33, ¼" Al.	11	88.9	402.	.26
B-33, 1/8" Al.	12	96.5	416.	.15
W-34, ¼" Al.	13	101.3	453.	.081

** Crystal Counter normalized

TABLE 8

RUN 36

NEUTRON ATTENUATION

SAMPLE ADDED	LOCATION NO.	TOTAL THICKNESS cm.	TOTAL THICKNESS gms/cm^2	SAT. CT. / MIN KW
1/4" Fe 1/4" Masonite	1	1.2	5.8	3.87×10^4
B-26, 1/8" Al 1/4" Masonite	2	7.3	17.7	736.8 (C)
B-25, 1/8" Al 1/4" Masonite	3	13.3	29.6	266.9
B-24, 1/8" Al 1/4" Masonite	4	19.4	41.4	106.1 (C)
B-23, 1/8" Al 1/4" Masonite	5	25.4	53.3	44.7
B-22, 1/8" Al 1/4" Masonite	6	31.4	65.2	20.7 (C)
B-21, 1/8" Al 1/4" Masonite	7	37.5	77.0	14.0
B-31, B-32, 1/4" Al 1/4" Masonite 1/2" Fe	8	54.2	116.9	0.99 (C)
B-33, B-34, 1/4" Al 1/4" Masonite	9	69.7	146.8	0.35
W-31, 1/4" Al 1/4" Masonite	10	75.4	184.7	0.51 (C)
W-32, 1/4" Al 1/4" Masonite	11	81.0	222.6	0.51
W-33, 1/4" Al 1/4" Masonite	12	86.7	259.9	0.34 (C)
1/2" Fe, W-34 1/4" Al, 1/4" Masonite	13	93.6	307.6	0.26
W-41, W-42, 1/2" Al 1/4" Masonite	14	103.3	377.3	0.041 (C)

TABLE 9 RUN 37

NEUTRON ATTENUATION

B_4C Paint, 1/4" Fe 1/4" Masonite	1	1.3	5.8	2.00×10^4 (C)
B-26, 1/8" Al W-21, 1/4" Al 1/4" Masonite	2	12.8	57.9	2.80×10^3
W-22, 1/4" Al 1/4" Masonite	3	18.9	98.9	1.56×10^3 (C)
W-23, 1/4" Al 1/4" Masonite	4	25.8	146.9	1.28×10^3 (C)
W-24, 1/4" Al B-25, 1/8" Al 1/4" Masonite	5	38.1	206.2	49.2
B-24, 1/8" Al 1/4" Masonite	6	44.1	218.0	13.3

RUN 37 (cont'd)

SAMPLE ADDED	LOCATION NO.	TOTAL THICKNESS cm.	TOTAL THICKNESS gms/cm^2	SAT. CT. / MIN KW
B-23, 1/8" Al 1/4" Masonite	7	50.2	229.9	3.92
B-22, 1/8" Al 1/4" Masonite	8	56.2	241.8	1.40
B-21, 1/2" Fe 3/8" Al, 3/4" Masonite Felt, B-31, B-32	9	79.6	294.4	.054
B-33, B-31 1/4" Al, 1/4" Masonite	10	95.1	324.33	.018
W-31, 1/4" Al. 1/4" Masonite	11	100.8	362.2	.029
W-32, 1/4" Al 1/4" Masonite	12	106.4	400.0	.024 (C)
W-33, 1/4" Al 1/4" Masonite	13	112.1	437.3	.022

(C) Cd covered foils.

Table 10 RUN 38

NEUTRON ATTENUATION

SAMPLE ADDED	LOCATION NO.	TOTAL THICKNESS cms	TOTAL THICKNESS gms/cm^2	SAT. CT./MIN.KW Au Foils No Cd	Au Foils Cd	W Foils No Cd	W Foils Cd
1/4" Fe, 2" Paraffin 1/4" Masonite	1	6.4	10.4	1.8×10^5	1.4×10^4	7.12×10^3	6.68×10^2
2" Paraffin B-26, 1/8" Al	2	16.2	26.0	20.2	–	0.65	-
2" Paraffin, B-25; 1/8" Al. 1/4" Masonite	3	27.9	42.3	1.91×10^3	232.3	98.8	10.4
2" Paraffin B-24, 1/8" Al	4	38.4	57.9	.61	---	----	---
2" Paraffin B-23; 1/8" Al. 1/4" Masonite	5	49.5	74.3	75.6	7.99	3.3	.42
B-22, 1/8" Al; 2" Para. 1/2" Masonite	6	61.3	91.5	.41	.35	.019	.016
1/4" Masonite 1/2" Fe B-31, 1/8" Al	7	70.6	116.8	.028	---	---	---
B-32, 1/8" Al 1" Wood 2" Paraffin 1/4" Masonite	8	86.3	138.5	2.9	.18	.098	---

TABLE 11 RUN 39

NEUTRON ATTENUATION

SAMPLE ADDED	LOCATION NO.	TOTAL THICKNESS		SAT. CTS. / MIN. KW
		cms.	gms/cm^2	
1/4" Fe	1	.6	5.0	52000
B-26, 1/8" Al	2	6.0	16.0	370
B-25, 1/8" Al	3	11.4	27.1	137
B-24, 1/8" Al	4	16.8	38.1	66
B-23, 1/8" Al	5	22.2	49.2	32.6
B-22, 1/8" Al	6	27.6	60.2	15.0
B-21, 1/8" Al	7	33.0	71.3	7.0

TABLE 12 RUN 40

NEUTRON ATTENUATION

SAMPLE ADDED	LOCATION NO.	TOTAL THICKNESS		TUNGSTEN FOILS (RED.CTS/MIN)	GOLD FOILS (SAT.CTS/MIN.KW)
		cms.	gms/cm^2		
1/4" Fe	1	.6	5.0	- -	1.41×10^6
B-22, 1/8" Al	2	6.0	16.0	4.05×10^4	817.
W-21, 1/4" Al	3	11.5	56.2	3.03×10^4	771.
W-22, 1/4" Al	4	16.9	96.4	2.52×10^4	640.
W-23, 1/4" Al	5	23.2	143.6	1.66×10^4	433.
W-24, 1/4" Al	6	29.5	191.0	8.49×10^3	188.
B-26, 1/8" Al	7	34.9	202.1	- -	41.0
B-25, 1/8" Al	8	40.3	213.1	- -	11.8
B-24, 1/8" Al	9	45.7	224.2	- -	4.1
B-23, 1/8" Al	10	51.1	235.2	- -	1.41
B-21, 1/8" Al	11	56.5	246.3	- -	3.10
1" cement 3/4" Masonite 1/4" Fe	12	61.60	258.8	- -	10.04

Table 13 RUN 41

NEUTRON ATTENUATION

SAMPLE ADDED	LOCATION NO.	TOTAL THICKNESS CMS.	TOTAL THICKNESS GMS/CM^2	SAT.CTS. / MIN.KW
1/4" Fe	1	.6	5.0	9.4×10^5
B-22, 1/8" Al	2	6.0	16.0	528.9
B-26, 1/8" Al 2" Paraffin	3	16.5	31.7	2.57×10^4
2" Paraffin B-25, 1/8" Al	4	27.0	47.3	5.2
B-24, 1/8" Al 2" Paraffin	5	37.5	62.9	532.
2" Paraffin B-23, 1/8" Al	6	47.9	78.5	.191
B-21, 1/8" Al 2" Paraffin	7	58.4	94.1	19.3
2" Paraffin 1/2" Fe B-31, 1/8" Al B-32, 1/8" Al 2"Paraffin	8	84.7	142.4	.679
2" Paraffin B-33, 1/8" Al B-34, 1/8" Al 2" Paraffin	9	109.7	180.6	.040

Table 14 RUN 42

NEUTRON ATTENUATION

1/4" Fe	1	.64	5.0	9.4×10^5
B-22, 1/8" Al	2	6.	16.0	297.
W-21, 1/4" Al	3	11.5	56.2	359.
B-21, 1/8" Al	4	16.9	67.3	179.
W-24, 1/4" Al	5	23.2	114.7	109.
B-24, 1/8" Al	6	28.6	125.8	43.1
W-22, 1/4" Al	7	34.0	165.9	27.0
B-25, 1/8" Al	8	39.4	177.0	11.7
W-23, 1/4" Al	9	45.7	224.2	6.7
B-26, 1/8" Al, 1/2" Fe	10	52.4	245.2	2.6
W-31, 1/4" Al	11	57.4	282.2	1.5
B-31, 1/8" Al	12	64.8	293.8	.38
W-32, 1/4" Al	13	69.8	333.8	.23
B 32, 1/8" Al	14	77.3	348.4	.065
W-33, 1/4" Al	15	82.3	384.9	.044
B-33, 1/8" Al	16	89.7	399.4	.012
W-34, 1/4" Al	17	94.7	436.3	.007
B-34, 1/8" Al	18	102.2	450.9	.010

Table 15

RUN 43

NEUTRON ATTENUATION

SAMPLE ADDED	LOCATION NO.	TOTAL THICKNESS CMS.	TOTAL THICKNESS GMS/CM^2	SAT. CTS. MIN. KW.
1/4" Fe, 1/4" Masonite	1	1.3	5.8	1.33×10^5
1/4" Wood, 1/4" Masonite 2" Paraffin	2	7.6	11.6	1.19×10^5
1/4" Masonite, 2" Paraffin	3	13.3	17.0	3.70×10^4
1/4" Masonite, 2" Paraffin	4	19.0	22.4	8.87×10^3
1/4" Masonite, 2" Paraffin	5	24.8	27.8	1.92×10^3
1/4" Masonite, 2" Paraffin	6	30.5	33.2	1.07×10^3
1/4" Masonite, 2" Paraffin	7	36.2	38.6	349.
1/4" Masonite, 2" Paraffin	8	41.9	44.0	117.
1/4" Masonite, 2" Paraffin	9	47.6	49.4	55.1
1/4" Masonite, 2" Paraffin	10	53.3	54.8	23.2
1/2" Wood, 1/4" Masonite 2" Paraffin	11	60.3	61.0	5.92
1/4" Masonite, 1/2" Fe	12	62.2	71.8	2.91
1" Wood, 1/4" Masonite 4" Paraffin	13	75.6	83.5	1.38
1" Wood, 2" Paraffin	14	83.2	89.9	0.78
3/4" Wood, 1/2" Paraffin	15	86.4	92.3	.60
1.18" Paraffin	16	89.4	95.0	.39
1.18" Paraffin	17	92.4	97.7	.27
1.18" Paraffin	18	95.4	100.4	.20
1.18" Paraffin	19	98.4	103.1	.11
1.18" Paraffin	20	101.4	105.8	.094
1.18" Paraffin	21	104.4	108.5	.093
1.18" Paraffin	22	107.4	111.2	.116

Table 16

RUN 45

NEUTRON ATTENUATION

SAMPLE ADDED	LOCATION NO.	TOTAL THICKNESS CMS.	TOTAL THICKNESS GMS/CM^2	54 Min Half Life	4.5 Hours Half Life	48 Days Half Life
1/4" Fe, B-25, 1/8" Al	1	6.0	16.0	2,223,500	38,215	809
B-26, 1/8" Al	2	11.4	27.1	859,600	18,331	326
B-24, 1/8" Al	3	16.8	38.1	453,940	10,929	168
B-21, 1/8" Al	4	22.2	49.2	224,160	3,754	92
B-22, 1/8" Al	5	27.6	60.2	107,440	2,374	50
B-23, 1/8" Al	6	33.0	71.3	54,788	1,184	22
1/2" Fe	7	34.3	81.3	39,572	974	17
B-32, 1/8" Al	8	41.7	95.8	13,384	377	7
B-31, 1/8" Al	9	49.1	110.4	4,836	153	2
B-33, 1/8" Al	10	56.6	124.9	1,655	72	1

Table 17

RUN 36

TRAVERSE DATA

SAT. CTS./ MIN. KW

Location	1	2	3	4	5	6	7	8	9	10	11	12	13	14
Position														
1	3.76×10^4	860C	341	163	68.3	34.2	25.6	2.35	.948	1.29	0.739	.733	.957	.121C
2	3.85×10^4	700C	243	100	41.8	21.0	13.5	1.05	.430	.70	0.554	.483	.357	.064C
3	3.18×10^4	618C	242	104	43.8	21.1	13.5	0.97	.362	.59	0.493	.412	.273	.046C
4	3.28×10^4	703	274	129	61.2	27.8C	20.9	2.57	.823	.85C	0.639	.542	.418	.083
5	4.80×10^4	615	201	83	36.5	16.3C	11.6	0.96	.410	.58C	0.521	.423	.306	.056
6	4.55×10^4	697	233	92	40.0	17.5C	11.8	0.91	.349	.50C	0.497	.383	.262	.047
7	4.09×10^4	741	255	106	44.0	19.7C	12.7	0.96	.352	.50C	0.504	.381	.255	.042
8	3.87×10^4	737C	267	106C	44.7	20.7C	14.0	0.99C	.347	.51C	0.505	.341C	.256	.041C
9	4.01×10^4	727	251	104	44.3	20.2C	12.9	0.98	.341	.50C	0.507	.367	.253	.041
10	4.23×10^4	665	226	94	39.6	18.0C	12.3	0.88	.335	.49C	0.506	.376	.248	.043
11	4.10×10^4	568	202	85	37.6	16.4C	12.2	0.94	.369	.53C	0.574	.380	.260	.045
12	2.66×10^4	815	336	160	71.7	29.7C	23.2	2.30	.646	.69C	0.763	.458	.327	.059
13	3.69×10^4	737C	260	104	45.4	21.4	13.7	0.96	.362	.56	0.535	.369	.249	.040C
14	3.48×10^4	674C	233	94	40.7	20.4	13.3	0.98	.391	.62	0.647	.396	.263	.043C
15	3.26×10^4	743C	290	130	62.2	33.6	24.9	2.26	.711	.96	1.004	.518	.354	.058C

[redacted]

RUN 37

Table 18

TRAVERSE DATA

SAT. CTS./ MIN. KW

Location	1	2	3	4	5	6	7	8	9	10	11	12	13
Position													
1	16.8×10^3C	3690	1515	1390	66.1	23.6	7.63	3.73	.213	.085	.098	.072	.049
2	17.8×10^3C	2530	1390	1170	37.5	10.9	3.48	1.28	.061	.026	.039	.036	.027
3	19.2×10^3C	2740	1625	1350	45.7	12.6	3.84	1.30	.055	.021	.030	.028	.026
4	-	2700	-	994C	56.3	21.4	9.69		.316	.076C	.097	.073	.048
5	-	2300	-	979C	36.7	11.7	3.82		.084	.033C	.056	.046	.034
6	-	2490	-	1115C	41.8	11.9	3.52		.053	.022	.036	.036	.025
7	-	2750	-	1270C	46.7	13.1	3.87		.052	.019	.030	.028	.022
8	20.0×10^3C	2800	1557C	1280C	49.2	13.3	3.92	1.40	.054	.018	.029	.024C	.022
9	-	2700	-	1260C	46.2	13.1	3.80		.052	.019	.030	.030	.023
10	-	2390		1100C	41.2	11.8	3.59		.053	.021	.037	.034	.028
11	-	2150	-	970C	36.6	11.6	3.75		.069	.032C	.054	.048	.037
12	-	2490	-	915C	65.7	23.5	9.59		.220	.066C	.097	.073	.053
13	19.7×10^3C	2700	1559	1340	46.9	13.5	3.80	1.36	.051	.021	.032	.029	.022
14	20.8×10^3C	2370	-	1150	40.6	12.1	3.75	1.44	.062	.029	.044	.041	.029
15	19.6×10^3C	2500	2048	1090	52.9	19.0	7.70	3.36	.188	.077	.093	.068	.047

[redacted]

[redacted]

Table 19

ORNL-435

RUN 38

TRAVERSE DATA

SAT. CTS./ MIN. KW

Location	1	2	3	4*	5	6	7	8
Position								
1	1.30×10^5	151.9	406.6C		320.6	10.1C	1.35	29.7
2	1.82×10^5	25.2	254.2C		150.2	2.0C	0.15	15.3
3	1.96×10^5	21.8	253.4C	1.74	81.4	.46C	.04	4.4
4	0.12×10^5C	69.9	1737.	0.71	14.8C	1.29	.14	0.60C
5	0.13×10^5C	21.0	1902.	0.71	9.4C	.51	.036	0.31C
6	0.14×10^5C	20.1	1968.	0.68	8.0C	.36	.101	0.18C
7W	668.0C	.62	99.0	0.66	.44C	.019		
8W	7123	.65	10.4C	0.61	3.3	.016C		.098
9W	669.0C	.64	98.6	0.64	.39C	.019		
10	0.14×10^5C	18.9	1852.	0.72	8.0C	.45	.025	.17C
11	0.12×10^5C	21.4	1902.	1.45	9.8C	.91	.042	.33C
12	0.16×10^5C	104.4	1980	.55	20.8C	3.90	.205	.66C
13	1.63×10^5	18.5	211.2C	.66	69.8	.24C	.016	1.3
14	1.49×10^5	17.7	195.4C		77.5	.33C	.020	1.8
15	1.05×10^5	46.4	249.3C		91.8	1.0C	.068	2.4

* -All these foils were gold and 4" apart.

[redacted]

RUN 39

Table 20 TRAVERSE DATA *

SAT. CTS./MIN. KW

Location	1	2	3	6	7
Position					
1	1202	23.12	12.25	1.77	3.54
2	1261	11.19	5.03	0.639	0.808
3	1270	9.81	4.04	0.492	0.398
4	1257	9.51	3.81	0.381	0.321
5	1295	9.60	3.64	0.349	0.251
6	1302	8.96	3.44	0.341	0.252
7	1222	8.40	3.39	0.329	0.243
8	1050	7.93	3.29	0.327	0.200
9	749	7.62	3.27	0.325	0.252
10	1035	8.13	3.25	0.318	0.228
11	1292	9.03	3.34	0.315	0.213
12	664	12.40	4.61	0.703	0.554
13	1084	6.63	2.49	0.342	0.209
14	1546	6.68	2.49	0.315	0.153
15	1539	7.20	2.57	0.322	0.147
16	1524	7.54	2.72	0.323	0.142
17	1481	7.80	2.87	0.335	0.153
18	1429	8.16	3.00	0.352	0.154
19	1403	8.27	3.10	0.363	0.158
20	1365	8.46	3.18	0.374	0.166
21	1343	8.73	3.18	0.356	0.166
22	1320	8.83	3.28	0.366	0.166
23	1327	9.15	3.33	0.397	0.174

24	1306	9.30	3.32	0.374	0.168
25	1303	9.26	3.42	0.375	0.176
26	1311	9.31	3.39	0.387	0.177
27	1320	8.82	3.42	0.429	0.182
28	1298	9.35	3.39	0.390	0.184
29	1297	9.27	3.34	0.424	0.181
30	1285	8.92	3.33	0.407	0.172
31	1277	9.02	3.35	0.430	0.181
32	1287	8.51	3.22	0.396	0.165
33	1279	8.89	3.16	0.319	0.164
34	1260	8.29	3.06	0.352	0.165
35	1241	8.21	2.91	0.357	0.163
36	1194	7.73	2.78	0.403	0.180
37		7.29	2.93	0.437	0.253
38	665	10.33	4.65	0.844	0.601
39	1297	9.27	3.43	0.312	0.204
40	1290	9.24	3.32	0.322	0.208
41	1231	8.72	3.24	0.312	0.223
42	1195	8.16	3.20	0.314	0.282
43	1146	8.03	3.10	0.306	0.214
44	1115	7.59	3.00	0.298	0.213
45	1103	7.64	2.89	0.298	0.214
46	1077	7.42	2.88	0.299	0.215
47	1080	7.53	2.71	0.317	0.253
48	1081	7.71	2.94	0.406	0.364
49	1035	11.03	4.81	0.735	0.798

* center: position 25; foils 1 cm apart; vertical traverse (up-down): positions 1-11, 25, 39-49; horizontal traverse: positions 12-38.

Table 21

RUN 40

TRAVERSE DATA

SAT. CTS./MIN. KW

I. Gold Foils

Location	2	3	4	5	6	7	9	11
Position								
1	1036.6		639.0		168.0	31.4	4.93	4.33
2	736.6		564.8		160.1	31.3	3.52	3.09
3	807.6	751.0	609.7	405.0	181.5	37.9	3.92	3.04
4	1617.9		528.7		142.8	35.2	5.87	4.82
5	692.4		507.7		141.3	29.0	3.47	3.16
6	738.0		541.9		157.7	33.6	3.60	2.89
7	792.9	747.9	608.0	402.3	179.5	38.9	3.99	3.00
8	817.0	770.9	639.6	432.9	187.7	41.0	4.19	3.10
9	795.5	752.9	606.7	411.4	204.2	39.1	4.05	3.05
10	739.3		561.3		162.9	34.2	3.61	2.81
11	712.5		536.8		148.8	29.2	3.36	2.85
12	1376.8		639.4		258.7	33.8	5.84	3.95
13	766.1	735.0	595.6	398.0	180.8	38.2	4.07	2.93
14	683.0		530.9		152.0	30.8	3.41	2.80
15	822.3		540.7		146.8	29.7	4.51	3.55

[redacted]

Table 21

TRAVERSE DATA

REDUCED CTS./MIN.

II. Tungsten Foils

Location	2	4	6
Position			
1	6.36×10^4	2.29×10^4	7.74×10^3
2	3.93×10^4	2.13×10^4	6.96×10^3
3	4.24×10^4	2.40×10^4	7.93×10^3
4	10.73×10^4	2.34×10^4	6.79×10^3
5	3.49×10^4	1.93×10^4	6.13×10^3
6	3.59×10^4	2.18×10^4	6.92×10^3
7	3.97×10^4	2.38×10^4	7.98×10^3
8	4.05×10^4	2.52×10^4	8.49×10^3
9	3.86×10^4	2.34×10^4	7.98×10^3
10	3.64×10^4	2.11×10^4	6.79×10^3
11	3.52×10^4	1.98×10^4	6.30×10^3
12	9.85×10^4	2.78×10^4	8.05×10^3
13	3.74×10^4	2.27×10^4	7.75×10^3
14	3.38×10^4	1.97×10^4	6.37×10^3
15	4.16×10^4	2.14×10^4	6.07×10^3

[redacted]

[redacted]

Table 22

RUN 41

TRAVERSE DATA

SAT. CTS./MIN. KW

Location	2	3	4	5	6	7	8	9
Position								
1	582.8	17,279	15.25	684.0	0.970	41.71	3.65	0.58
2	482.9	22,048	6.02	589.8	0.296	35.86	1.72	0.16
3	531.2	25,382	5.36	546.8	0.204	22.07	0.82	0.06
4	1159.4	15,721	19.77	538.9	0.969	39.76	3.50	0.47
5	452.5	19,966	5.62	581.0	0.274	35.64	2.91	0.25
6	488.6	21,690	4.83	492.1	0.191	22.35	1.10	0.070
7	521.6	24,433	5.11	516.2	0.184	19.35	0.70	0.044
8	528.9	25,675	5.20	532.5	0.191	19.34	0.68	0.040
9	519.3	25,186	5.17	524.6	0.190	19.50	0.73	0.043
10	493.2	22,690	5.03	513.2	0.205	20.79	0.93	0.058
11	453.0	20,208	5.37	567.9	0.275	25.83	1.57	0.13
12	878.2	15,250	15.25	471.7	1.406	23.78	1.89	0.20
13	503.5	23,675	4.75	484.2	0.176	18.32	0.68	0.041
14	449.5	19,786	4.48	462.4	0.180	19.48	0.96	0.07
15	638.6	15,768	7.33	411.4	0.375	21.13	1.53	0.15

[redacted]

[redacted]

ORNL-435

Table 23

RUN 42

TRAVERSE DATA

SAT. CTS./MIN.KW

Location	3	6	9	12	15	18
Position						
1	580.42	33.69	9.55	1.23	0.411	0.061
2	341.21	24.87	6.21	.40	0.064	0.022
3	351.40	26.49	6.40	.38	0.045	0.011
4	429.20	29.14	7.21	1.49	0.265	0.023
5	302.27	21.57	5.44	.41	0.074	0.013
6	310.44	23.82	5.62	.35	0.045	0.010
7	344.47	26.23	6.33	.37	0.044	0.010
8	358.94	26.99	6.66	.38	0.044	0.010
9	349.88	25.82	6.50	.38	0.045	0.012
10	326.36	23.57	5.97	.36	0.042	0.012
11	320.78	23.24	6.01	.38	0.060	0.013
12	450.49	36.59	9.75	.91	0.190	0.017
13	334.16	25.19	6.35	.37	0.043	0.011
14	301.39	22.10	5.68	.35	0.047	0.010
15	365.81	25.30	6.39	.86	0.161	0.013

[redacted]

RUN 43

Table 24 TRAVERSE DATA

SAT. CTS./MIN. KW

Location	2	5	8	13	15*	16*	21*	22*
Position								
1	87,022.	2591.	354.8	16.19				
2	119,464.	2312.	216.9	7.01				
3	119,026.	1985.	126.3	2.13				
4	84,173.	2406.	220.0	8.30				
5	125,163.	2240.	205.4	5.84				
6	128,670.	1913.	144.4	2.79	4.858	1.199	0.245	0.922
7	120,560.	1897.	121.9	0.74	1.319	0.453	0.0918	0.179
8	119,245.	1922.	117.1	1.38	0.604	0.389	0.0932	0.116
9	120,560.	1937.	117.4	1.54	0.781	0.447	0.108	0.0734
10	117,272.	2095.	141.0	2.72	2.049	1.367	0.296	0.241
11	109,162.	2562.	232.8	7.58				
12	79,350.	2869.	311.8	9.81				
13	114,422.	1794.	112.7	1.51				
14	102,366.	1838.	150.0	3.43				
15	79,789.	2264.	206.9	6.83				

* Foils 4" apart.

[redacted]

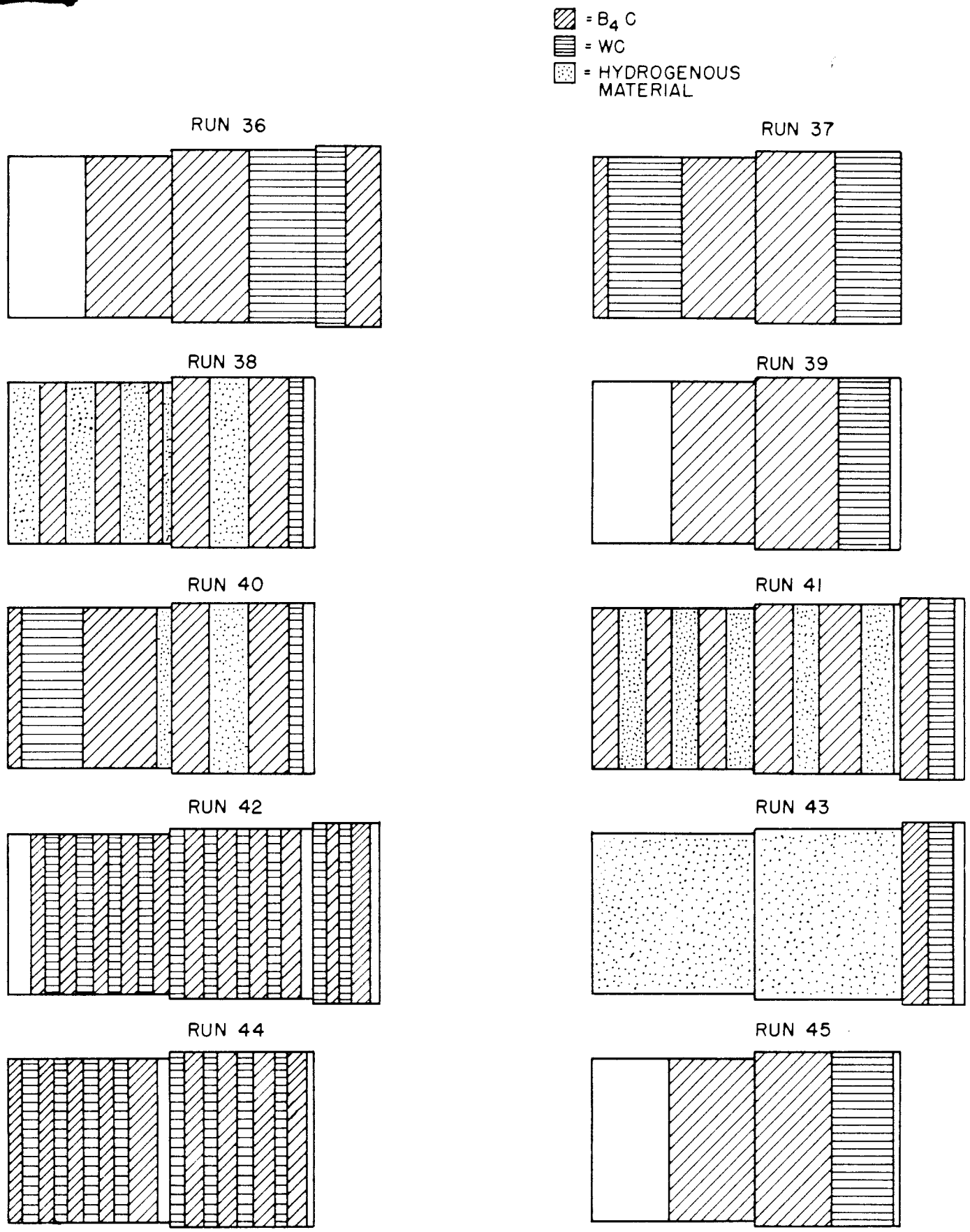

GEOMETRIES NEPA SHIELDING TESTS

[redacted]

FIG. 2 PAGE 59

GAMMA ATTENUATION

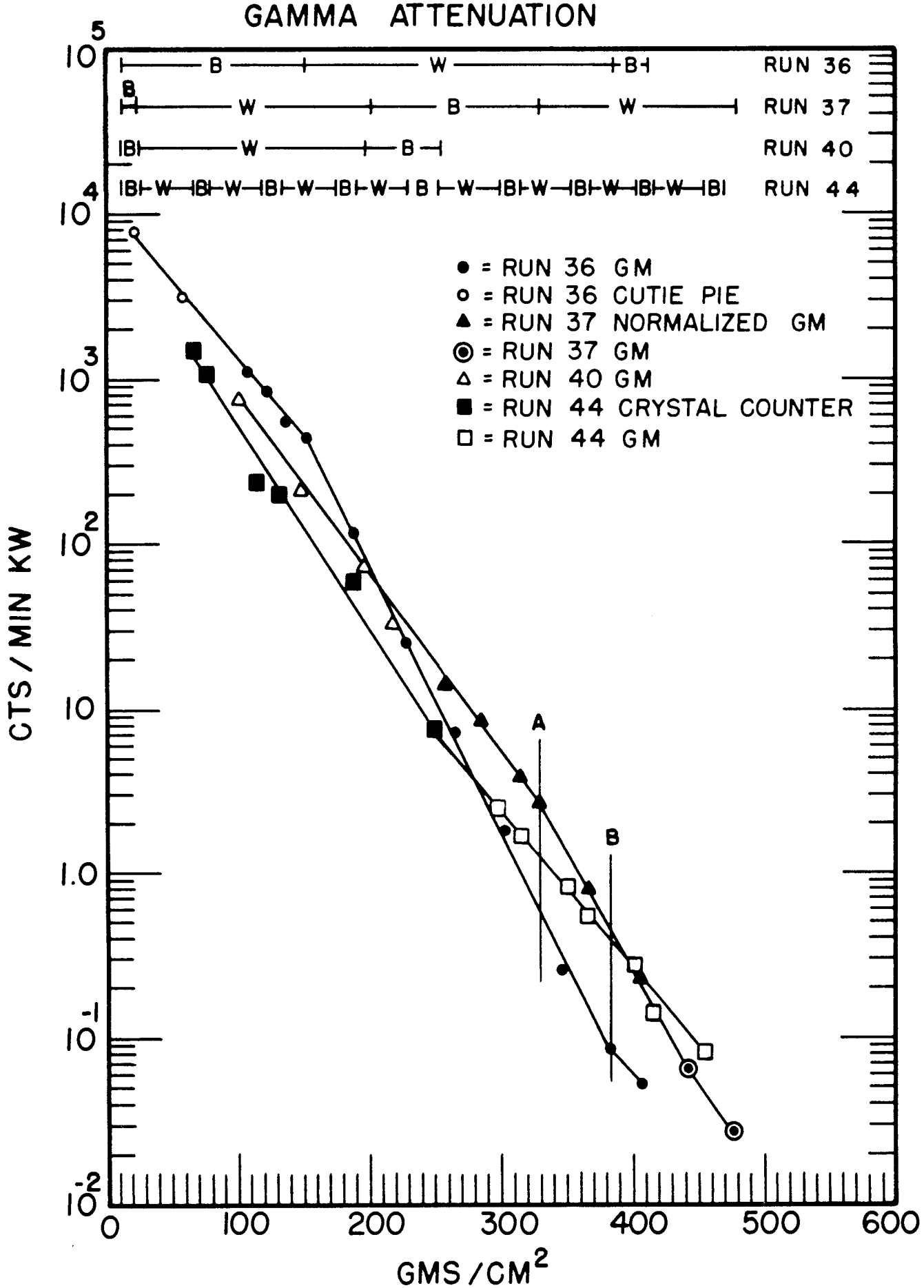

[redacted]

NEUTRON ATTENUATION

FIG. 3 PAGE 60

Dr. 7823

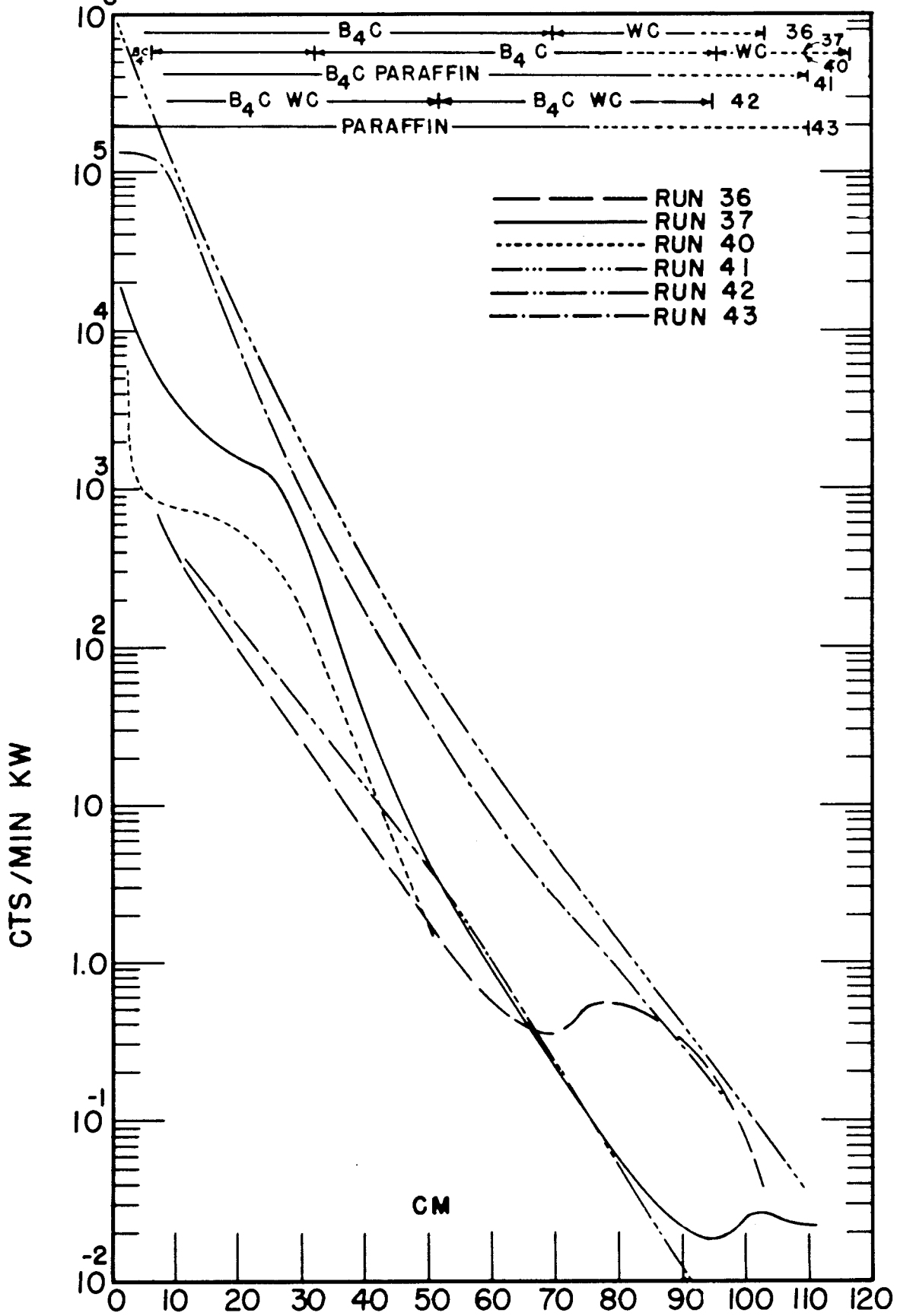

[redacted]

FIG. 4 PAGE 61

Dr. 7824

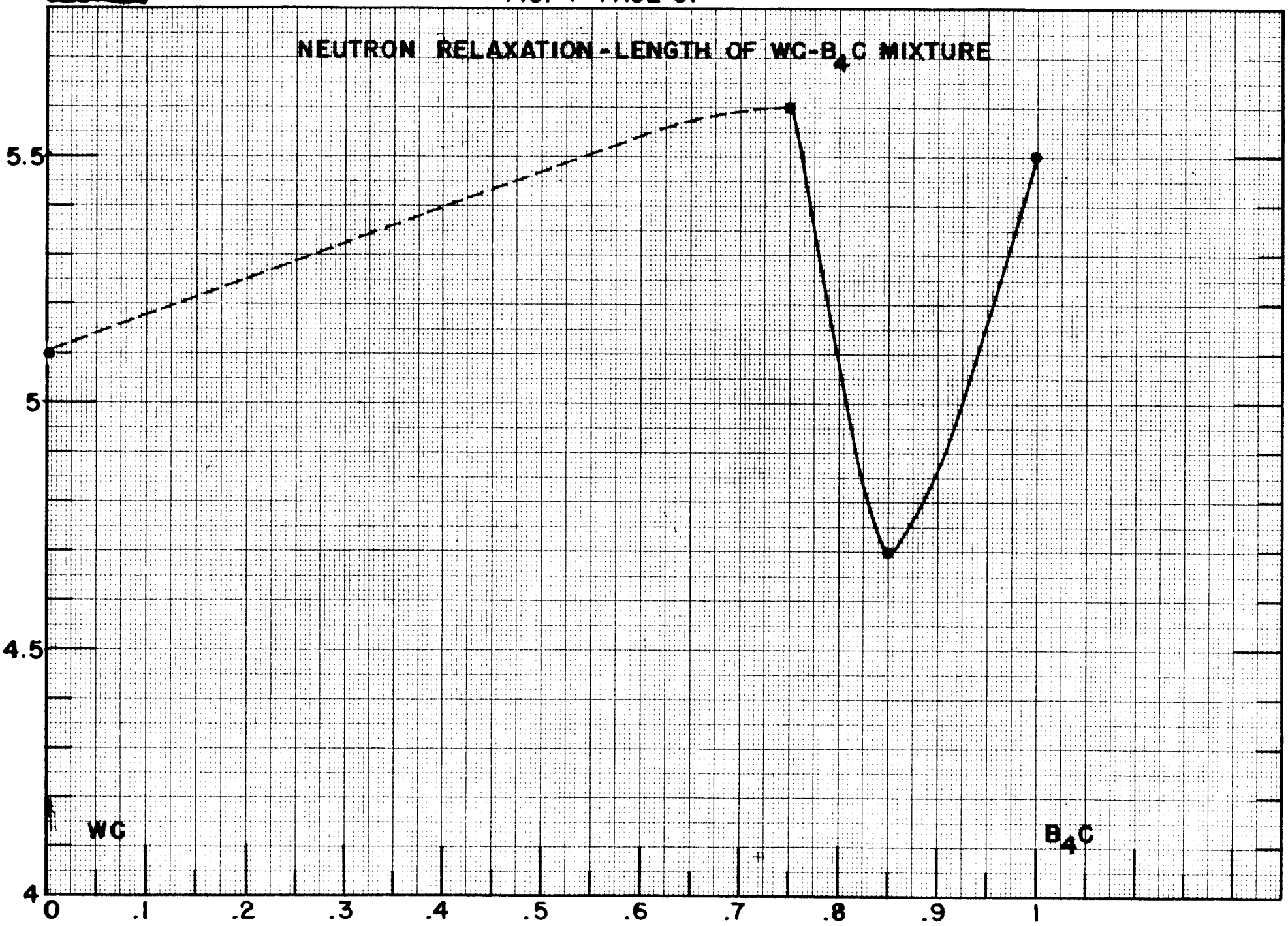

[redacted]

FIG. 5 PAGE 62

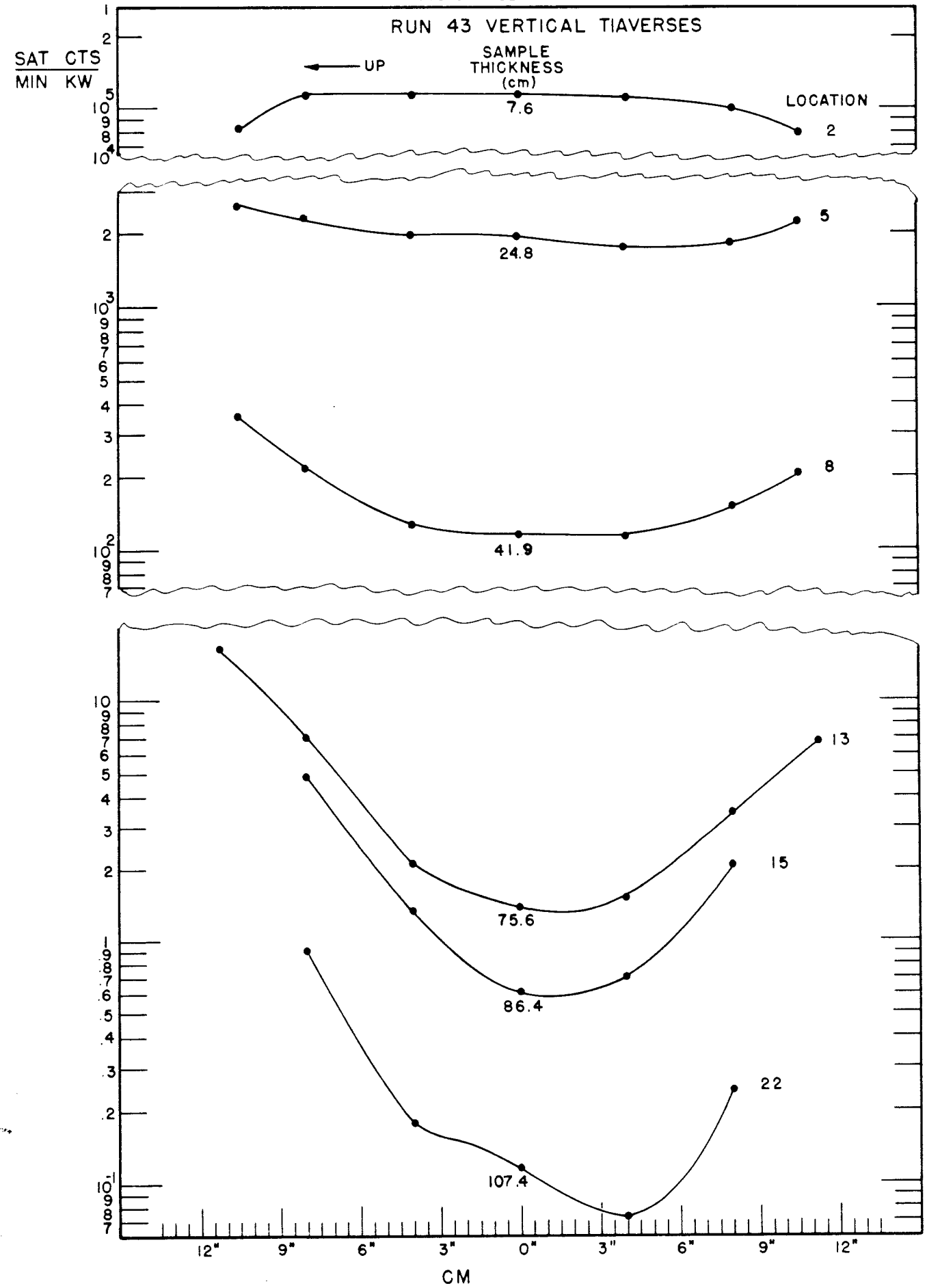

[redacted]

Dr. 7450

TRANSPORT BOXES

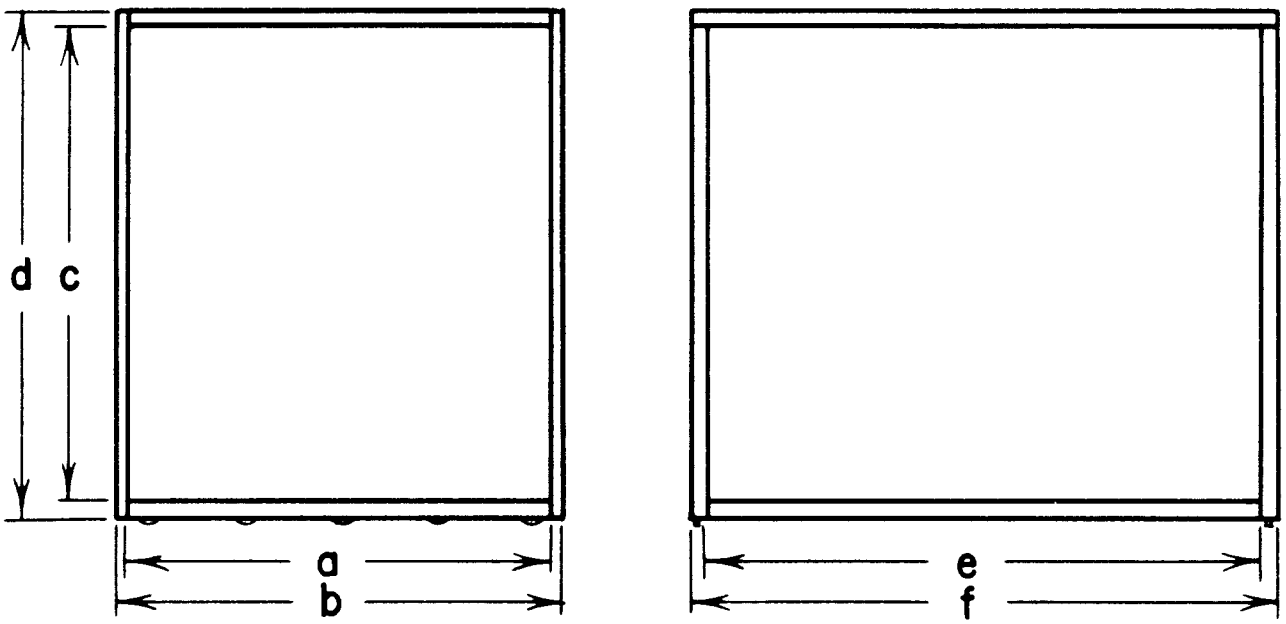

Box No. / Dimension	2	3	4
a	24 7/8"	21 3/4"	9 9/16"
b	25 3/8"	22 1/4"	10 1/16"
c	23 3/4"	25 1/4"	27"
d	25	26 1/2"	28 1/4"
e	27 11/16"	29 1/8"	30 13/16"
f	28 15/16"	30 3/8"	32 1/16"

FIG. 6 PAGE 63

FRAMES

Dr. 7451 [redacted]

FIG. 7

page 64

Frame No.	a	b	c*) inches	c*) cm	g/cm² *)	A	B	C	D	E	F	G
B-21	27.5	23.7	2.01	5.12	9.9							
B-22	27.5	23.7	2.00	5.07	9.9							
B-23	27.5	23.7	2.00	5.09	10.0							
B-24	27.5	23.7	2.00	5.09	9.7							
B-25	27.5	23.7	2.01	5.12	9.9							
B-26	27.5	23.7	2.01	5.12	9.7							
B-31	29.0	25.2	2.80	7.12	13.3							
B-32	29.0	25.2	2.81	7.15	13.6							
B-33	29.0	25.2	2.80	7.10	13.5							
B-34	29.0	25.2	2.80	7.12	13.6							
B-41	30.7	26.8	2.00	5.09	9.7							
B-42	30.7	26.8	2.95	7.48	14.2							
W-21	27.6	23.7	1.91	4.85	38.1	3½	3½	3½	3½	6½	None	5
W-22	27.6	23.7	1.90	4.83	38.0	4	4	4	4	6	used	6
W-23	27.6	23.7	2.22	5.64	45.1	4	3½	5	4	6		6
W-24	27.6	23.7	2.24	5.69	45.3	4½	3½	5½	4½	6		5½
W-31	29.0	25.2	1.72	4.37	34.9	4	3½	5	4	6	6 3/4	7
W-32	29.0	25.2	1.72	4.37	34.9	4½	3½	5	4½	6	6 3/4	7
W-33	29.0	25.2	1.73	4.39	34.4	4	4	4½	6	5	6 1/2	5
W-34	29.0	25.2	1.73	4.39	34.8	4½	3	4½	4½	6	6 1/4	6
W-41	30.7	26.8	1.52	3.86	32.3	5	4½	5	5	6	3 5/8	6½
W-42	30.7	26.8	1.52	3.86	32.4	5½	4	5½	5½	6	3 3/8	6

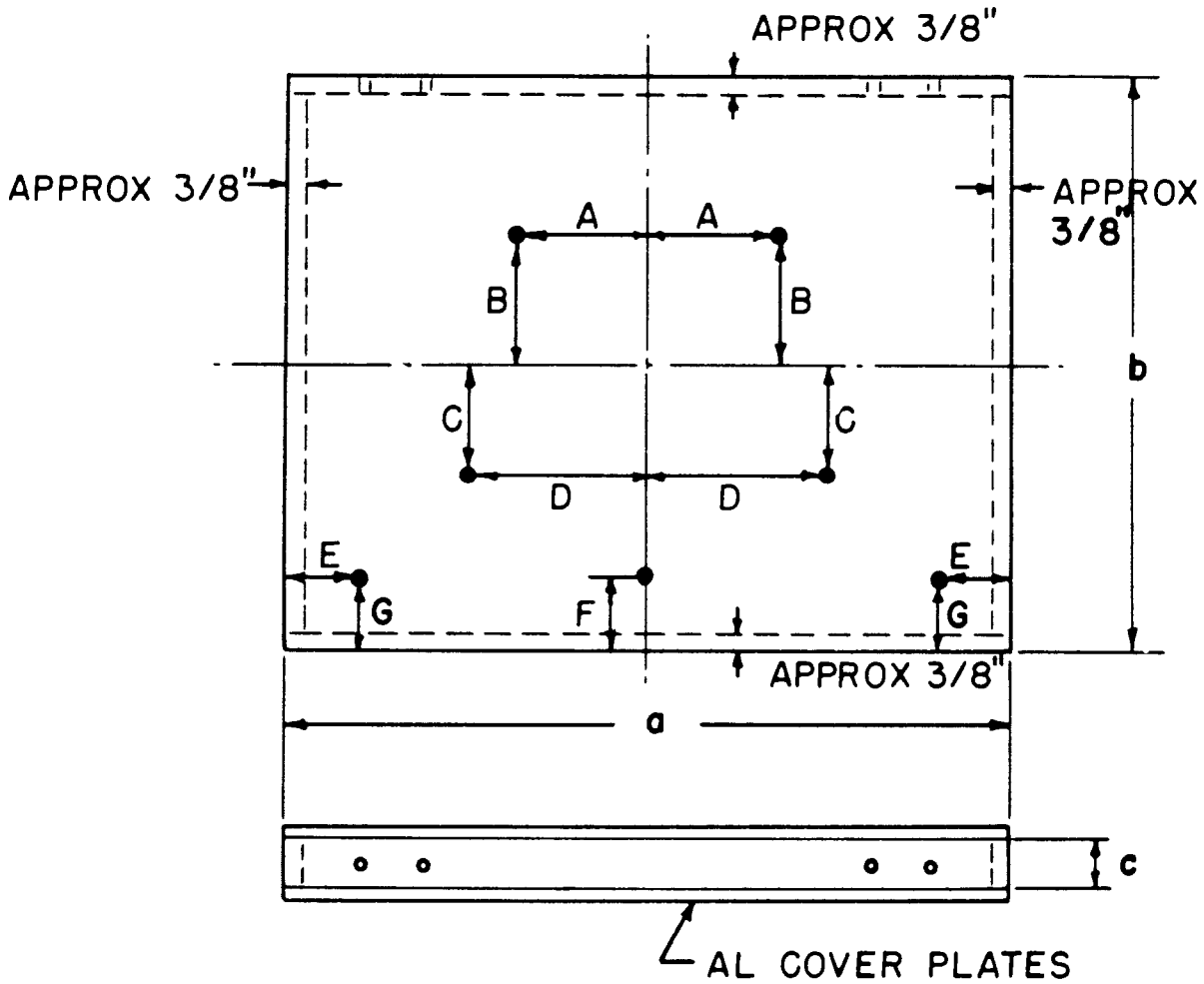

*) Does not include Aluminum cover plates.
These totaled 1/8" = 0.32 cm, or 0.86 g/cm² for each B_4C frame, and ¼" = 0.63 cm or 1.71 g/cm² for each WC frame.

[redacted]

Dr. 6637

(REVISED)

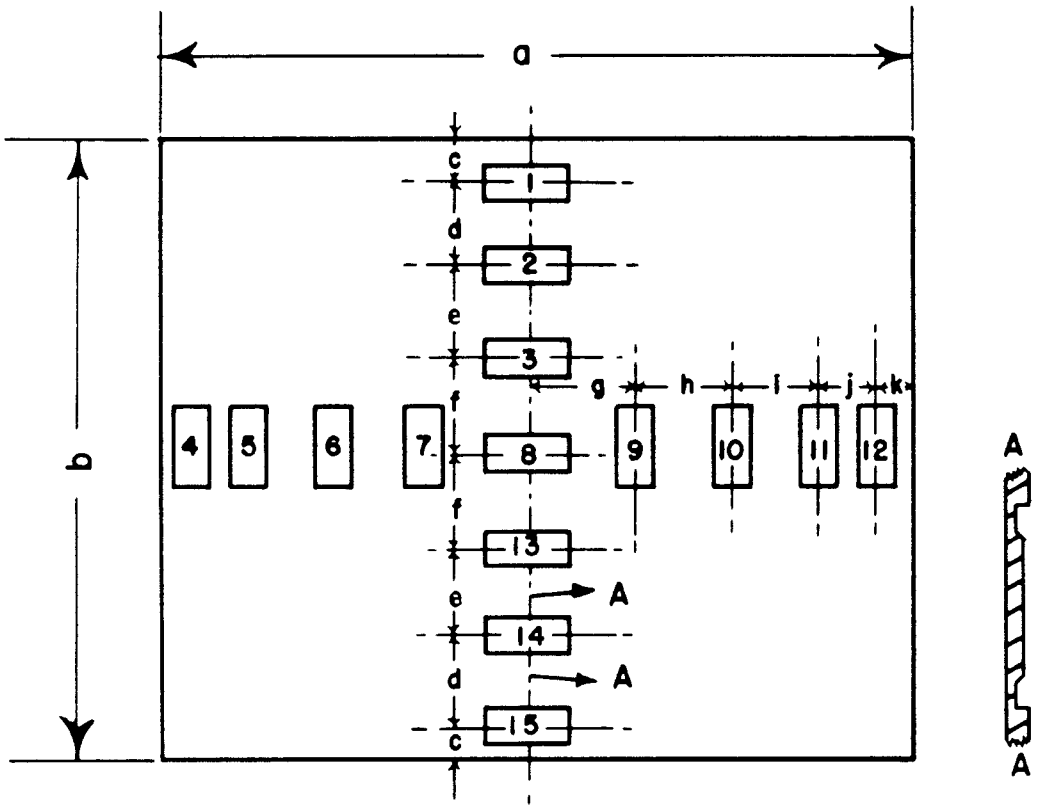

HOLDER SIZE	a	b	c	d	e	f	g	h	i	j	k
2	$27\frac{1}{2}$	$23\frac{3}{4}$	$1\frac{3}{8}$	$2\frac{1}{2}$	4	4	4	4	$2\frac{7}{16}$	$2\frac{1}{4}$	$1\frac{1}{16}$
3	29	$25\frac{1}{4}$	$1\frac{1}{2}$	$3\frac{1}{8}$	4	4	4	4	$3\frac{3}{16}$	$2\frac{3}{16}$	$1\frac{1}{8}$
4	$30\frac{3}{4}$	$26\frac{3}{4}$	$1\frac{3}{8}$	4	4	4	4	4	4	$2\frac{3}{16}$	$1\frac{3}{16}$

FIG. 8 PAGE 65

[redacted]

FIG. 9 PAGE 66

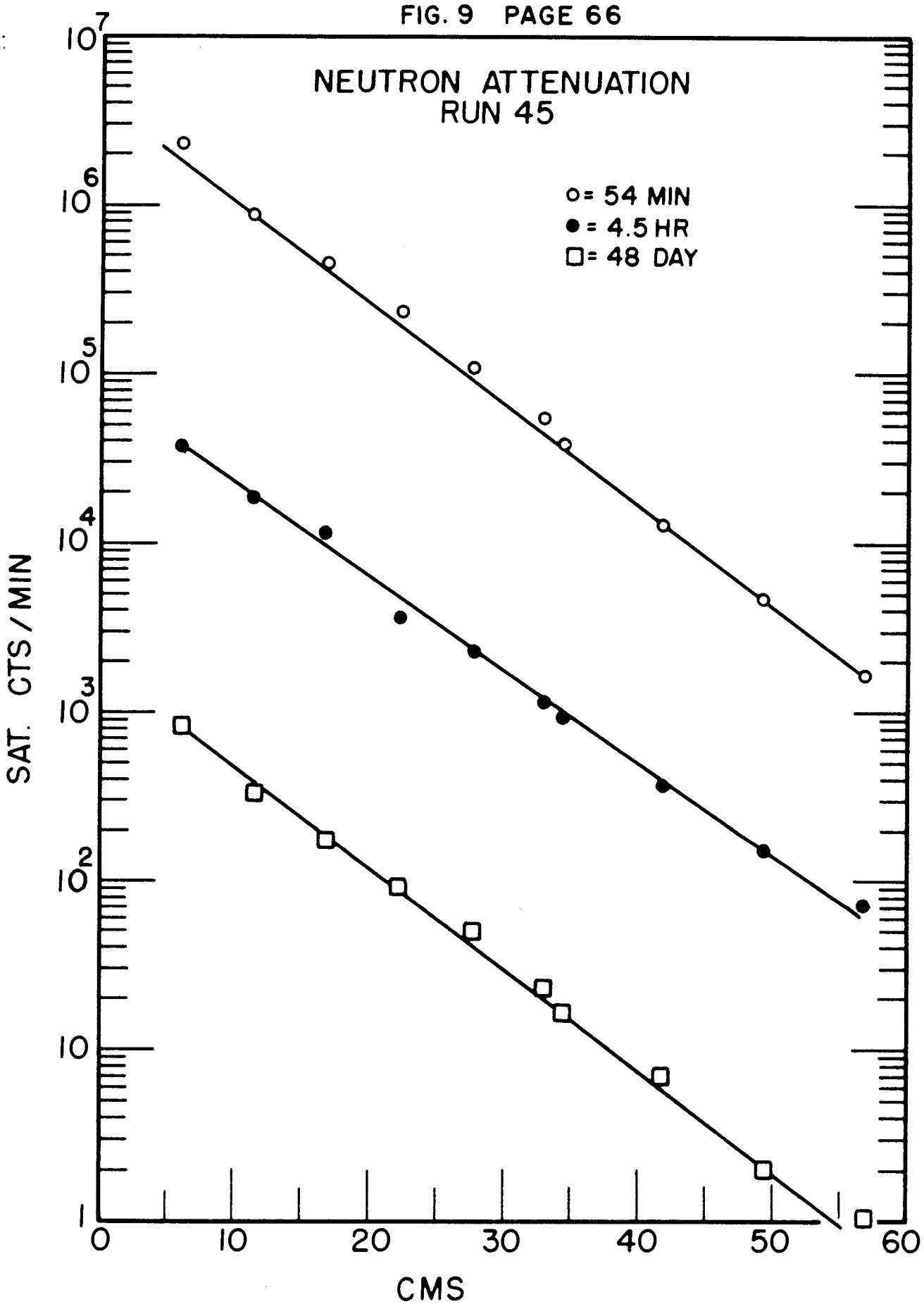

[redacted]

Dr. 7827

MODEL

FIG. 10 PAGE 67

DATE

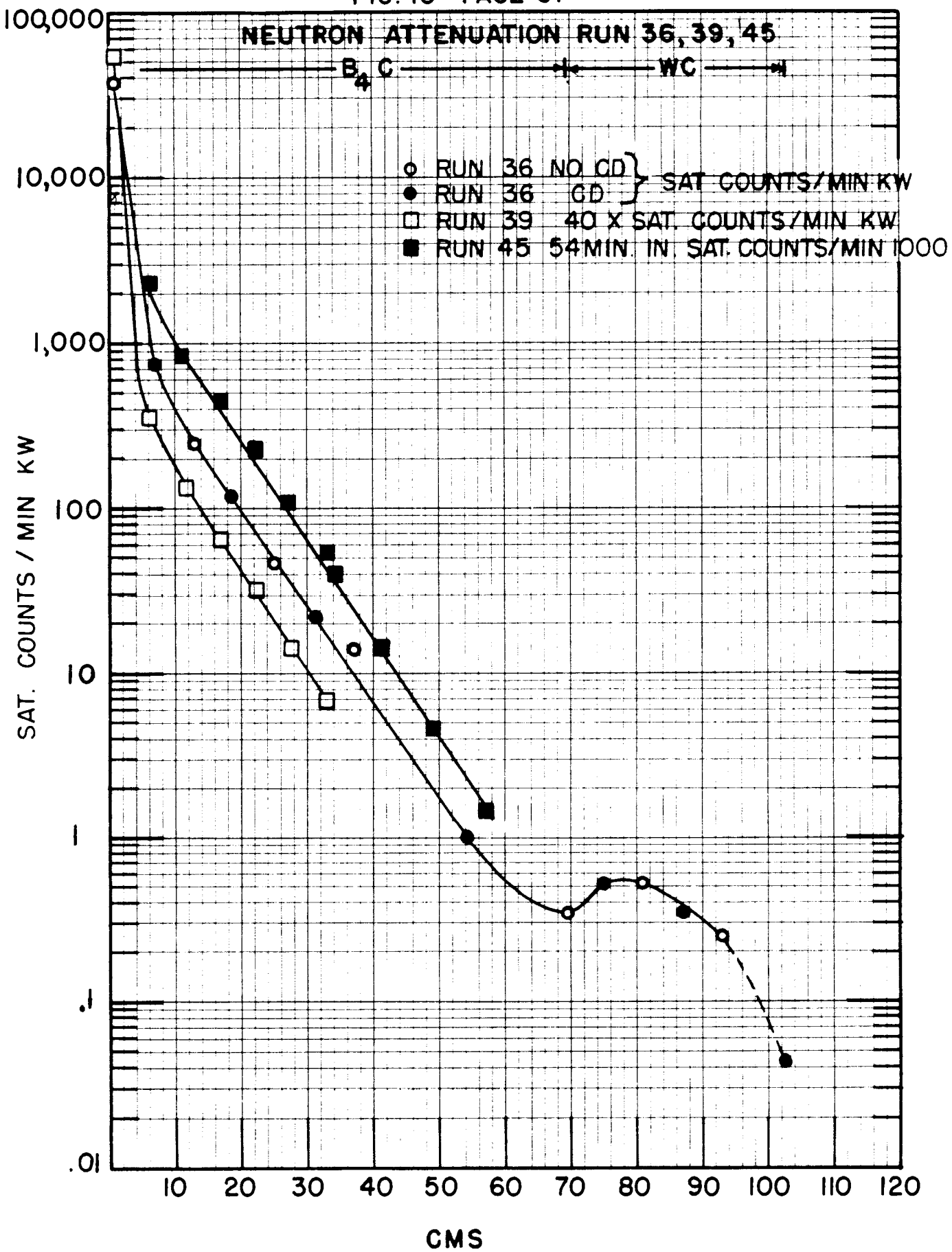

[redacted]

NEUTRON ATTENUATION
RUN 37 - RUN 40
FIG. 11 PAGE 68

Dr. 7828

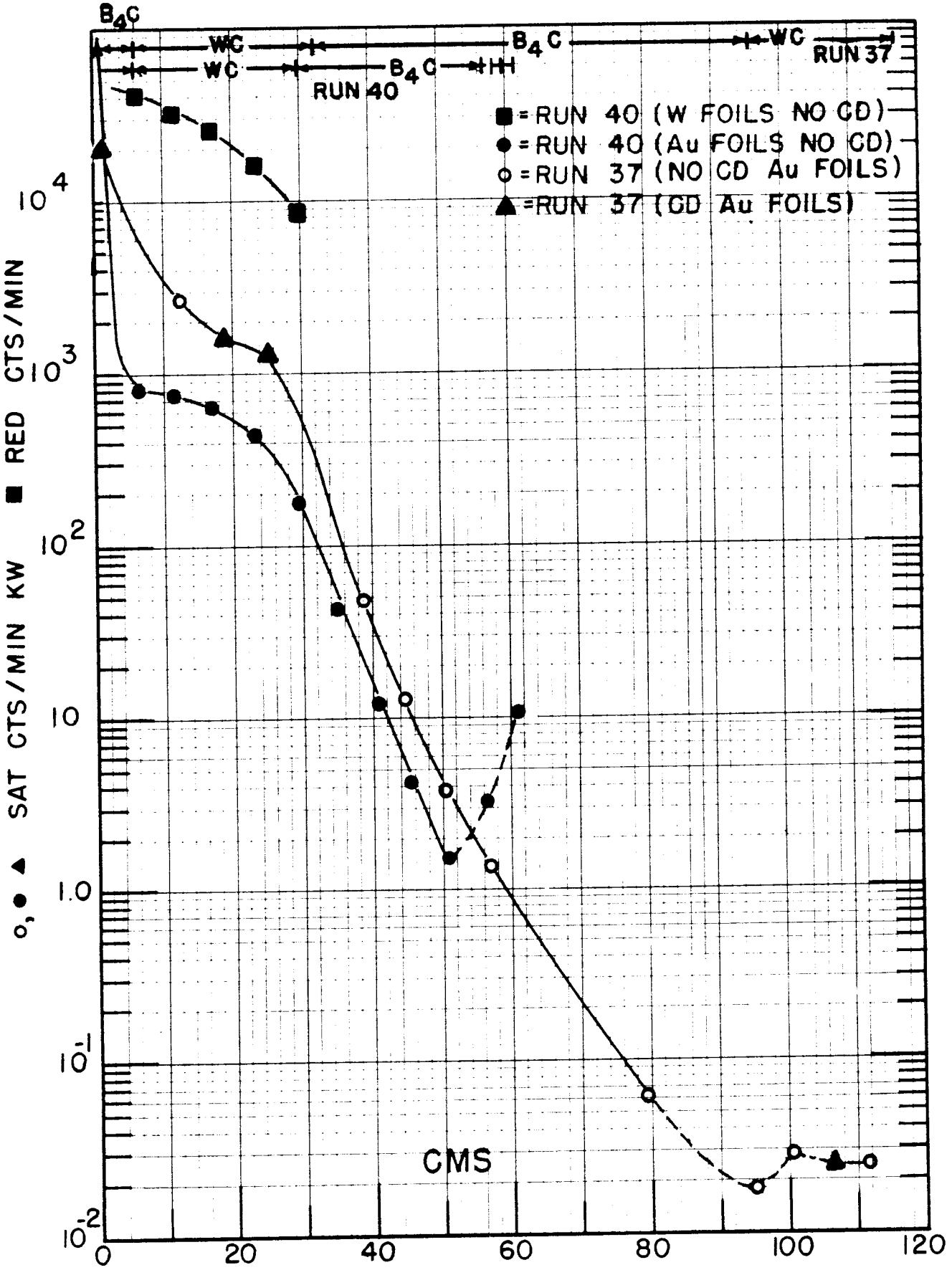

[redacted]

FIG. 12 PAGE 69

Dr. 7829

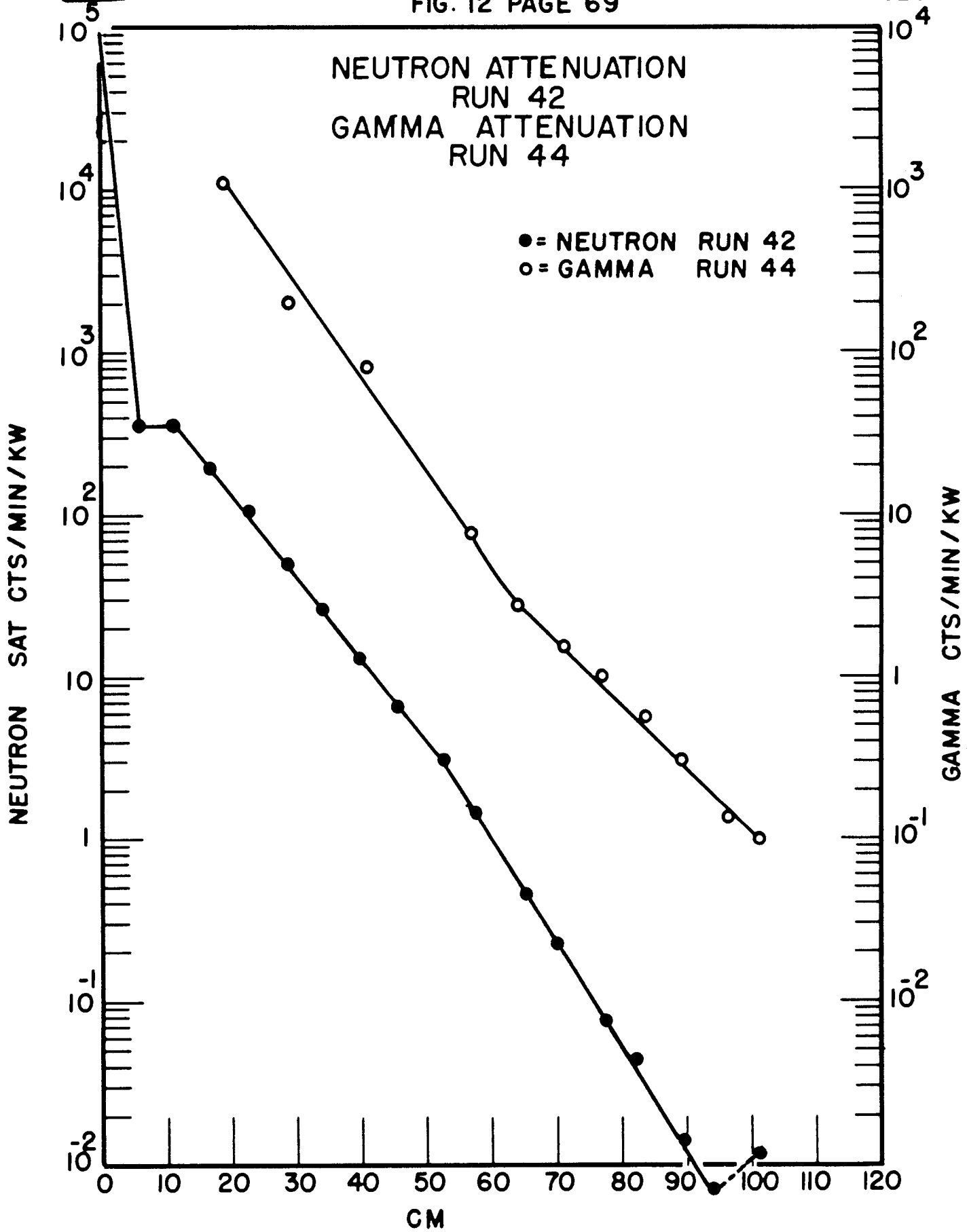

[redacted]

FIG. 13 PAGE 70

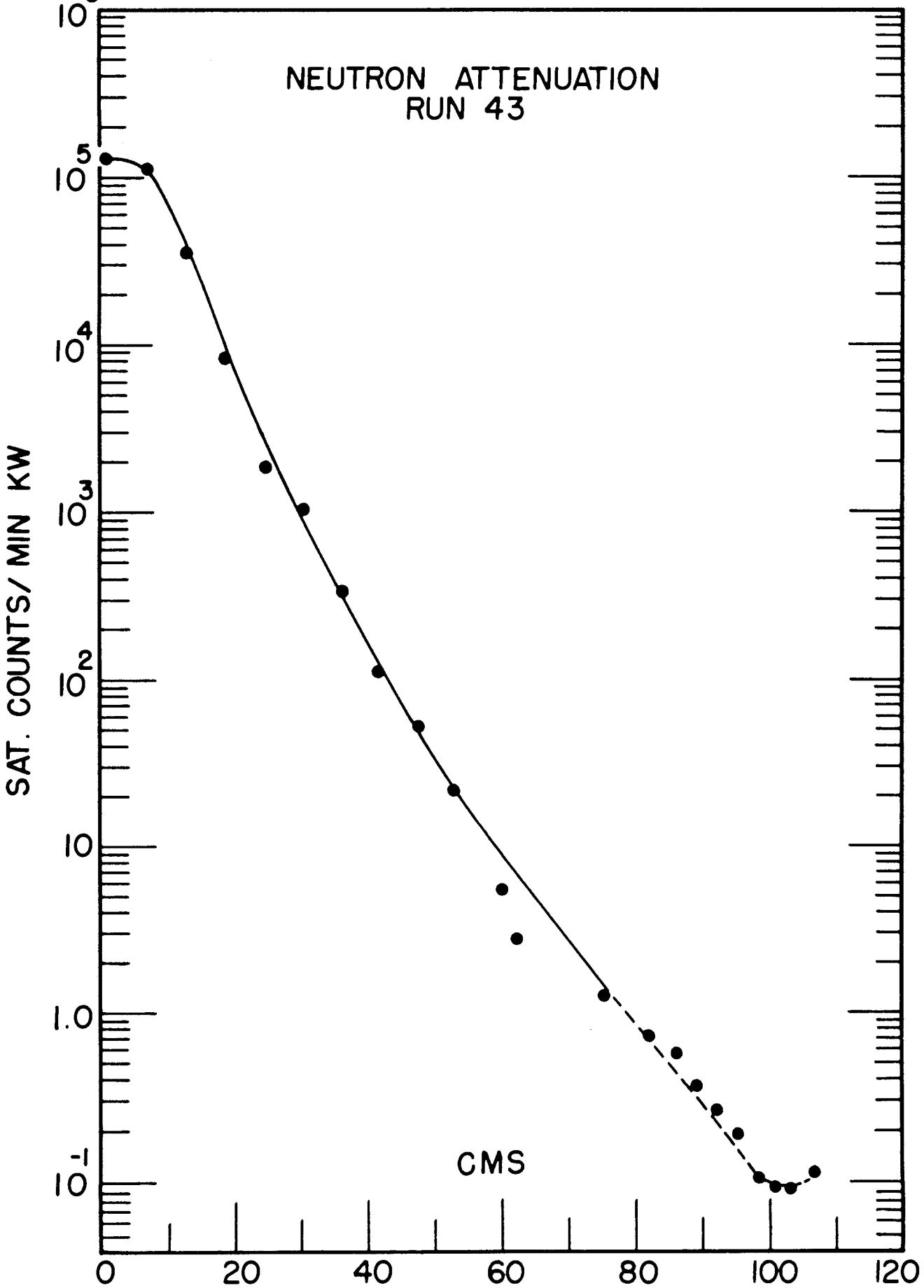

[redacted]

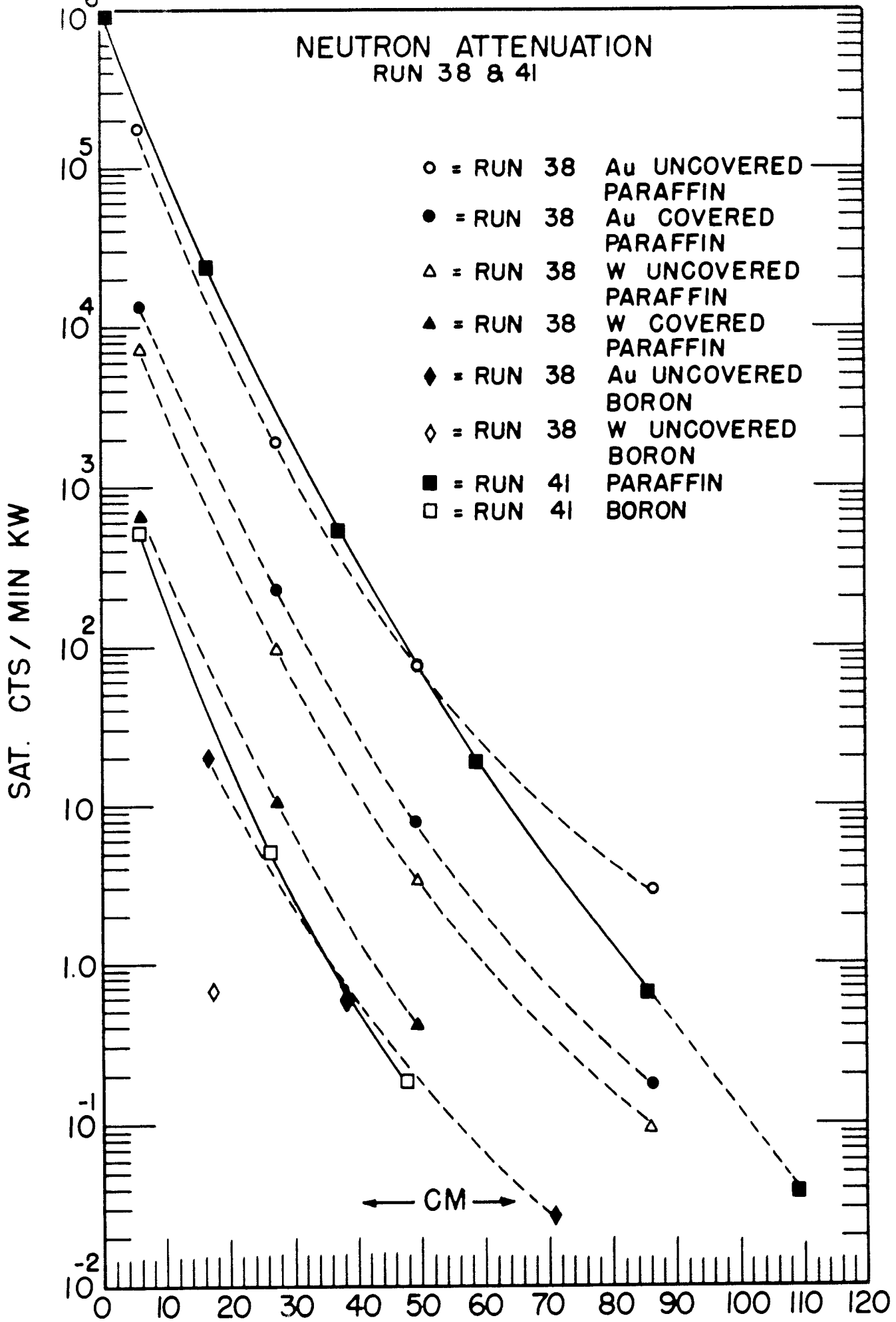
NEUTRON ATTENUATION
RUN 38 & 41
○ = RUN 38 Au UNCOVERED PARAFFIN
● = RUN 38 Au COVERED PARAFFIN
△ = RUN 38 W UNCOVERED PARAFFIN
▲ = RUN 38 W COVERED PARAFFIN
◆ = RUN 38 Au UNCOVERED BORON
◇ = RUN 38 W UNCOVERED BORON
■ = RUN 41 PARAFFIN
□ = RUN 41 BORON
SAT. CTS / MIN KW
10^6
10^5
10^4
10^3
10^2
10
1.0
10^{-1}
10^{-2}
0
10
20
30
40
50
60
70
80
90
100
110
120
CM

[redacted]
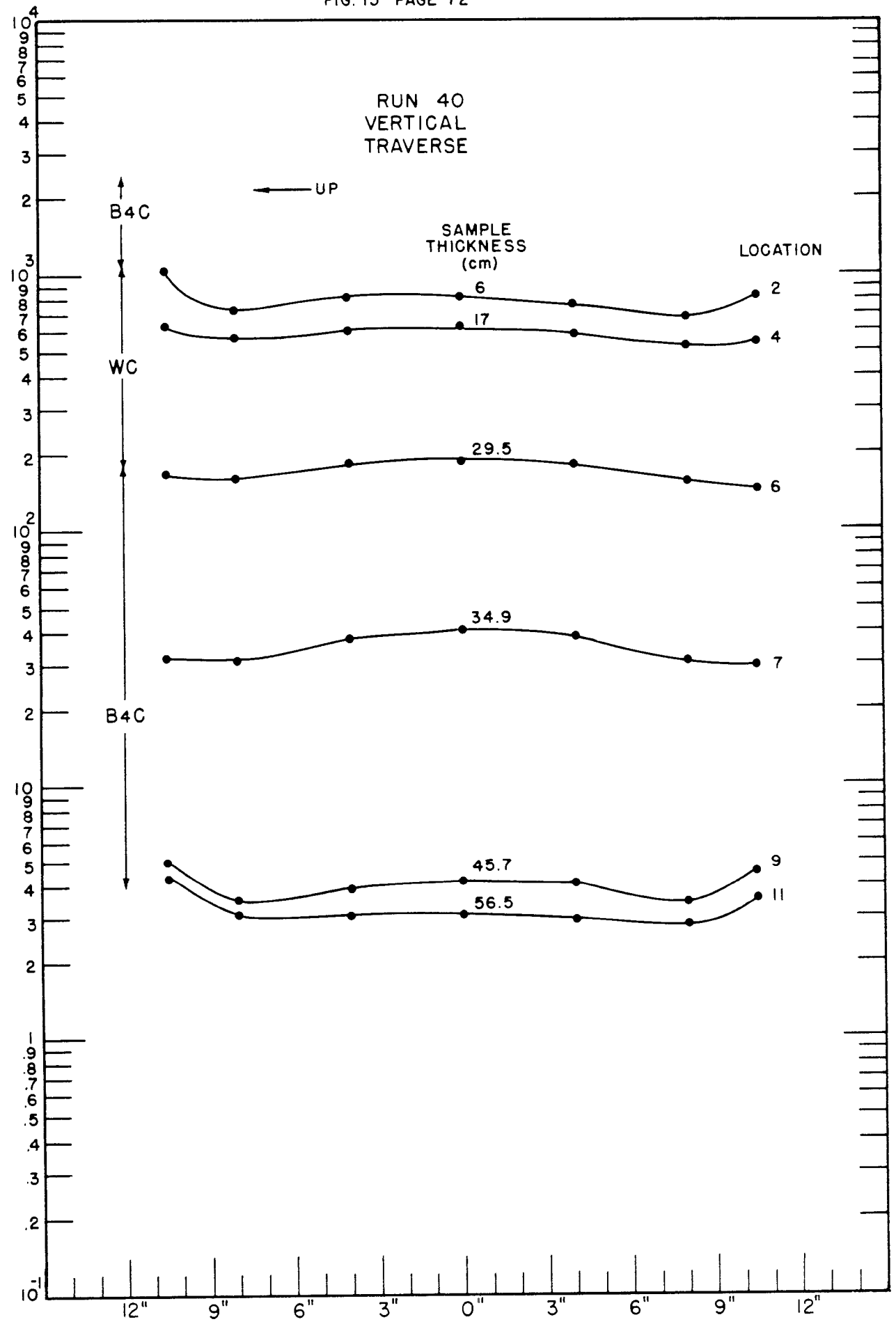
FIG. 15 PAGE 72